TOWARDS BETTER USER CUSTOMIZATION OF LOWER-LIMB ASSISTIVE DEVICES: DATA DRIVEN CONTROL STRATEGIES AND A SELF-ALIGNING KNEE MECHANISM

A Dissertation

by

NAMITA ANIL KUMAR

Submitted to the Graduate and Professional School of
Texas A&M University
in partial fulfillment of the requirements for the degree of

DOCTOR OF PHILOSOPHY

Co-Chairs of Committee,	Pilwon Hur
	Prabhakar Pagilla
Committee Members,	Reza Langari
	Xudong Zhang
Head of Department,	Guillermo Aguilar

December 2021

Major Subject: Mechanical Engineering

ABSTRACT

Despite the advances made in the field of lower-limb assistive walking devices, user customization of such devices remains a challenge. This work proposes three novel solutions towards addressing this challenge. Conventional walking controllers for transfemoral prostheses require tedious tuning of 12-20 control parameters per joint. Moreover, these parameters would have to be re-tuned when the terrain's slope angle changes. The first contribution of this dissertation is a new control framework that develops a set of relationships based on the correlation between the control parameters and the progress in the gait cycle. These relationships, also called joint parameter functions, were determined through data-driven approaches. Implementation of these functions greatly reduced the number of tuning parameters to 3-6 per joint. For the second contribution, this framework was extended to sloped walking by determining a mapping from the slope angle to the necessary joint parameter functions. While these solutions help improve user-customization of prostheses controllers, the mechanical design limitations of assistive devices must also be addressed. The polycentricity of human joints like the knee hinders user customization of assistive walking devices. State-of-the-art knee orthoses mechanisms result in a rotation axis mismatch between the user's knee and the device. Such mismatch leads to device migration and high interaction forces. The final contribution of this dissertation is a novel self-aligning knee mechanism suitable for a diverse group of users, easing user-customization.

DEDICATION

To stubborn hardware,

Rest in pieces when I'm done.

Time is closing fast.

ACKNOWLEDGMENTS

I sincerely thank my committee: Dr. Pilwon hur, Dr. Prabhakar Pagilla, Dr. Reza Langari, and Dr. Xudong Zhang. Ph.D. is not a smooth journey and they served as beacons all the way till finish line. I thank the graduate advisors, Rebecca Simons and Angela Montez, for answering every dumb question I had about my graduate studies. My sincere thanks to Sandra Havens for all the support and pep talks. She is the heart and soul of the Mechanical Engineering Department, and should be treated like a queen. I extend my gratitude to Dr. James Hubbard, Dr. Alan Palazzolo, and Dr. Joanna Tsenn for all the advice and encouragement. I also thank Drew Hubbard for helping me during the last leg of my journey.

I am grateful to my dear friend and colleague, Shawanee' Patrick, for being my guide runner and pulling me up when I stumbled. My heartfelt thanks to Woolim Hong for all the late nights spent trying to make stubborn hardware work. I also extend my gratitude to all other members of the Human Rehabilitation Group, specifically, Chistian DeBuys, Moein Nazifi, Kenneth Chao, and Yi-tsen (Amy) Pan. None of this would have been possible were it not for Kenny Chour. In him, I have found a lifelong friend. He has my undying gratitude. Finally, I thank my family for their unwavering support and love. They have been my pillar of strength throughout my journey. Thank you, Amma and Anna.

CONTRIBUTORS AND FUNDING SOURCES

Contributors

This work was supported by a dissertation committee consisting of Professor Pilwon Hur and Professor Prabhakar Pagilla of the Department of Mechnical Engineering and Professor Reza Langari from the Department of Engineering Technology and Industrial Distribution and Professor Xudong Zhang from the Department of Industrial and Systems Engineering.

The code implementation in Chapter III and IV was conducted with the help of Woolim Hong. Data collection and subject recruitment for Chapter III, IV, and V were done in collaboration with Shawanee' Patrick. The experiment design in Chapter V was conducted in part by Shawanee' Patrick. All listed contributors are from of the Department of Mechanical Engineering. Results presented in Chapter III and IV were published at IEEE ICRA 2020 and 2021 conference respectively with the aid of Woolim Hong.

All other work conducted for the dissertation was completed by the student independently.

Funding Sources

Graduate study was supported by several fellowships from Texas A&M University: Charles Crawford Fellowship for the years 2019, 2020, and 2021; Walker Impact Award, 2020.

TABLE OF CONTENTS

Page

LIST OF FIGURES

FIGURE Page

LIST OF TABLES

TABLE Page

1. INTRODUCTION

A 2016 study showed that 28% of the US population suffer from walking disabilities [1]. About 1.3 million are lower limb amputees [2] while the others suffer from spinal cord injuries limiting their ability to walk [3]. Despite decades of research in the field of human rehabilitation, the usage of powered walking assistive devices remains viable only in academic or therapeutic centers due to numerous challenges. Setting aside the more obvious challenges like battery limitations and the bulkiness of motors, a challenge that is less addressed is the difficulty in customizing the assistive walking devices to the user. This chapter discusses the limitations of the current state-of-the-art and outlines this dissertation's goals to improve current lower-limb walking assistive devices. This work tackles three problems related to user customization of said devices in dedicated chapters. Each chapter presents an extensive literature review and highlights the research gap. Accordingly, a hypothesis is formulated, and objectives are laid towards proving the same. The rest of each chapter explains the methods involved and discusses the associated results. The current chapter will serve as an overview of the proceeding ones, tying together all contributions under a common cause.

1.1 State-of-the-art of lower-limb assistive devices and their limitations

With prosthetics, energetically passive devices are the only commercially available solutions. An energetically passive device stores and dissipates energy without providing net positive work to the gait cycle. The lacking positive work is compensated for by the user's residual limb, which overexerts the hip and pelvic muscles and eventually leads to severe gait asymmetries [4]. Powered prostheses, on the other hand, provide a net positive work and consequently lower a user's metabolic cost [5, 6]. The Ossur Power knee is the only powered prosthesis currently on the market; it is known to not work well with middle aged and older users [7], and while walking on sloped terrains [8, 9]. There are no commercially available powered knee and ankle prostheses. The ones studied are limited to academic settings [10, 11, 12, 13, 14, 15, 16, 17, 18, 19]. The lack

of technology transfer from academia to industry can be attributed to several factors, with some being: (i) Limited battery capacity, (ii) poor weight-to-torque ratio of current motor technology, and (iii) the complexity of tuning each controller to different users. While many are working towards overcoming the first two challenges, little attention has been paid to the last factor.

Victims of spinal cord injuries form a targeted market for orthoses and exoskeletons. Several research groups, focusing on developing powered lower-limb exoskeletons, have made major strides towards ensuring stable walking with the aid of crutches [20, 21, 22, 23]. With considerable progress being made with the design of exoskeletons, clinical studies were naturally conducted to evaluate the efficacy, safety, and ergonomics of the designs. A European study conducted at various rehabilitation centers revealed that extensive usage of exoskeletons led to ankle swelling and pressure sores [24]. It is believed that the straps used to affix the exoskeleton to the user induce shear and ultimately lead to pressure sores [25, 26]. Another commonly reported complaint is the extensive amount of time required to don the exoskeleton. Additionally, several sessions are necessary to fine-tune adjustments and ensure a fit to the subject [25]. In other words, the process of customizing exoskeletons to a user's biomechanics and preferences is currently tedious and takes extensive time.

1.2 User customization of assistive walking devices

As noted earlier, a major challenge is the limited customization of devices to the user's needs and wants. Device customization requires changes to both control and mechanical design, resulting in long fitment and tuning time. Customization of control systems has seen minor contributions with the most significant being the implementation of machine learning for auto-tuning level walking controller's parameters [27]. The lack of contributions on this topic is primarily due to the problem's sheer magnitude. Since each mode of operation (e.g. standing, walking, stair ascent or descent) has its own control law, user customization of the control system involves tuning an unmanageable number of tuning parameters. Even walking on differently sloped terrain requires re-tuning the control law. At this point, any solution that simplifies this behemoth of a task is appreciated. This work tackles two problems:

Problem 1: Conventional level walking control strategies for powered transfemoral prostheses require tuning anywhere from 12 to 20 parameters.

Problem 2: The control law for sloped walking must be manually tuned for each slope angle and user preference.

Regarding mechanical customization of prosthetics, many have actively pursued the issue of user customization and have proposed various solutions like customized sockets, adjustable height, and foot stiffness [28, 29, 30, 31, 32]. But mechanical customization of orthoses and exoskeletons is not trivial. The primary challenge is the polycentricity of human joints. The human knee is not simple a pin joint since the femur rotates and slides on the tibia, as the knee flexes or extends. This results in a joint with a varying center of rotation. At any time, the joint's axis is termed as the Instantaneous Center of Rotation (ICR) and the locus of the ICR is called a centrode. Exoskeleton joint designers typically desire the joint's axis to be coincident with the user's knee axis. Any misalignment between the device's joint axis and the user's knee axis can lead to increased interaction forces and device migration [33]. Designing an exoskeleton joint that accurately mimics this polycentric action is a difficult task, which is further compounded by the fact that the centrode is unique to the user. While some contributions have been made to solve this issue [34, 35, 36, 37, 38, 39, 40, 41], these proposed solutions have not been compared to the state-of-the-art, bringing into question the effectiveness of the contributed solutions. Thus, the third problem tackled in this dissertation is:

Problem 3: The mismatch between the user's and exoskeleton's centrode leads to device migration and long donning time.

1.3 Hypotheses and structure of the dissertation

The objective of this dissertation is to solve the previously listed three problems. The solutions and their underlying hypotheses form the contributions of this dissertation. Before delving into solutions, there is a need to understand the basics of human biomechanics which has been briefly discussed in Chapter 2. The chapters that follow detail solutions to the three problems. Each

problem has an associated hypothesis and a list of objectives. For Problem 1, it is hypothesized that there a mathematical mapping between the gait progression and control law parameters. This mapping will be called control parameter functions. If proven true, implementation of the hypothesized mapping can significantly reduce the number of tuning parameters. Chapter 3 details this hypothesis and tests the same. Furthermore, this hypothesis can be used to solve Problem 2. As mentioned earlier, the control parameters must vary with the slope angle. Currently, there exists no framework relating the control parameters and the slope angle. The second hypothesis is that there exists a mapping between the control parameter functions (from the first hypothesis) and the slope angle. Such a mapping would enable designing controllers for any given slope angle. This hypothesis has been proven and tested in Chapter 4. For the final problem, it is hypothesized that a mechanism with built-in compliance allows self-alignment with any user's centrode. Such a self-aligning mechanism would reduce donning time, device migration, and interaction forces between the device and the user. Details pertaining to this hypothesis are given in Chapter 5.

2.1 Overview of the human gait cycle

The gait cycle is characterized by a heel-strike to another heel-strike on the same limb. All measurements therein are mapped to 0%-100% regardless of the walking speed and slope (refer Fig. 2.1)> Some important instants in the gait cycle are heel-strike ($\phi_{HS} \equiv 0\%$) to flat-foot (ϕ_{FF}), flat-foot (ϕ_{FF}) to heel-off (ϕ_{HO}), heel-off (ϕ_{HO}) to toe-off (ϕ_{TO}), and toe-off (ϕ_{TO}) to the end of the gait cycle (100%). Terrain adaptation generally occurs between ϕ_{HS} and ϕ_{FF}. Load transference from the trailing to the leading limb occurs during the period ϕ_{FF} to ϕ_{HF}. The lower limb joints perform mostly negative work during this section of the gait cycle. The period ϕ_{HO} to ϕ_{TO} is called the push-off section. During this period, all joints release stored energy, providing the human with the necessary propulsive work to move forward. ϕ_{FF} and ϕ_{HO} are assumed to be the instant when the foot stops and starts accelerating respectively. Toe-off (ϕ_{TO}) is assumed to occur when the ground reaction force (the normal force at the foot) drops below 10% of the human's weight.

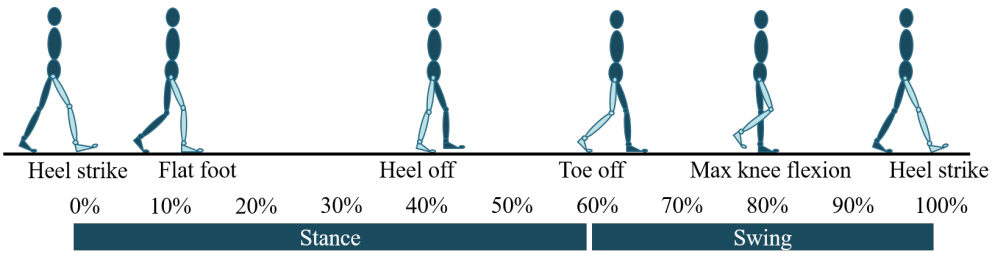

Figure 2.1: Gait cycle with import kinematic kinematics moments

The percentage of the gait cycle at which the above instants occur depend on the walking speed and the terrain's slope. The following section discusses slope-induced changes in detail. Some key gait kinematic and kinetic aspects while walking at different walking speeds have been listed here. Since this work's goal is to design a controller for a transfemoral prosthesis, this chapter's

discussion is limited to the knee and ankle joint. The highlighted points will be used to evaluate the controller's performance. The following increase with walking speed: (i) ankle dorsiflexion during mid and terminal stance, (ii) ankle plantarflexion during push-off, (iii) push-off torque and work, (iv) knee flexion during initial stance, (v) knee flexion torque during initial stance, (vi) knee extension torque during push-off. An important reference for level walking healthy human data is [42].

2.2 Human gait kinematics and kinetics on slopes

Useful resources for sloped walking include: a $n = 20$ study by [43], a $n = 10$ study by [44] which also has a publicly available data-set [45]. The study [43] presents data for 7 slope angles (-9° to $+9^\circ$ at 3° increments), while the study [45] presents results for 9 slope angles (-10° to $+10^\circ$ at 2.5° increments). The proceeding sections discuss the kinematics and kinetics of sloped walking.

2.2.1 Kinematics

Some important kinematic aspects of sloped walking are as follows. (i) The switching conditions of a finite state machine (shown in Figure 2.1) change with the slope and walking speed. The instant of flat-foot (ϕ_{FF}) and heel-off (ϕ_{HO}) tend to occur earlier as the slope angle varies from steep downslope to steep upslope. On the other hand, toe-off (ϕ_{TO}) is delayed as the slope varies (Refer Figure 2.2). (ii) The amount of ankle plantar-flexion at toe-off increases as the slope varies from steep downslope to steep upslope. (iii) The ankle angle at the beginning of the gait cycle changes with the slope angle to facilitate terrain adaptation. E.g., the ankle is more dorsiflexed on inclined slopes. (iv) The amount of knee-flexion during initial stance phase increases with the steepness of the slope be it upslope or downslope.

2.2.2 Kinetics

The most important trends in sloped walking kinetics are: (i) the increase in push-off peak ankle torque and power as the slope varies from steep downslope to upslope (ii) more knee flexion torque during stance on steeper slopes. These trends are more strictly obeyed in [43], while the data

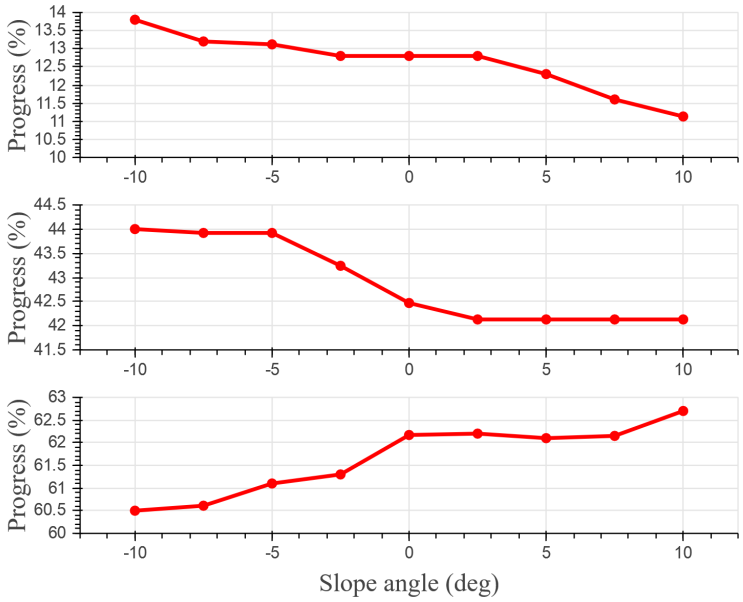

Figure 2.2: The variation in the stages of the gait cycle as a function of the slope's angle. **Top:** Flat-foot, **Middle:** Heel-off, **Bottom:** Toe-off.

pertaining to $-5°$, $-2.5°$ in [45] deviate from said trends. In fact, the entire downslope walking torque data from [45] is higher than that found in [43] by a factor of 1.3-1.5. It is believed [43] is more accurate owing to the larger sample size. On the other hand, the data in [45] spans more slope conditions which helps greatly while determining the relationship between control parameters and the slope angle. This work continues to use the data from [45], keeping in mind some anomalies are to be expected during downslope walking. These anomalies will be accounted for during implementation and the final proposed control scheme with be accordingly adjusted.

2.3 Nature of human joints

The sliding and rotating motion of the knee can be modeled as a four-bar mechanism. Upon studying X-ray images of the knee, the study [46] estimated the link lengths of the four-bar system. Figure. 2.3 depicts a simplified model of the knee featuring the four-bar mechanism. It shows the knee in both an extended and flexed state. It must be emphasized that these lengths are estimates and will likely differ between individuals. But this model serves as a good example for demonstrating the limitations of current knee orthoses and exoskeletons detailed in Chapter 5.

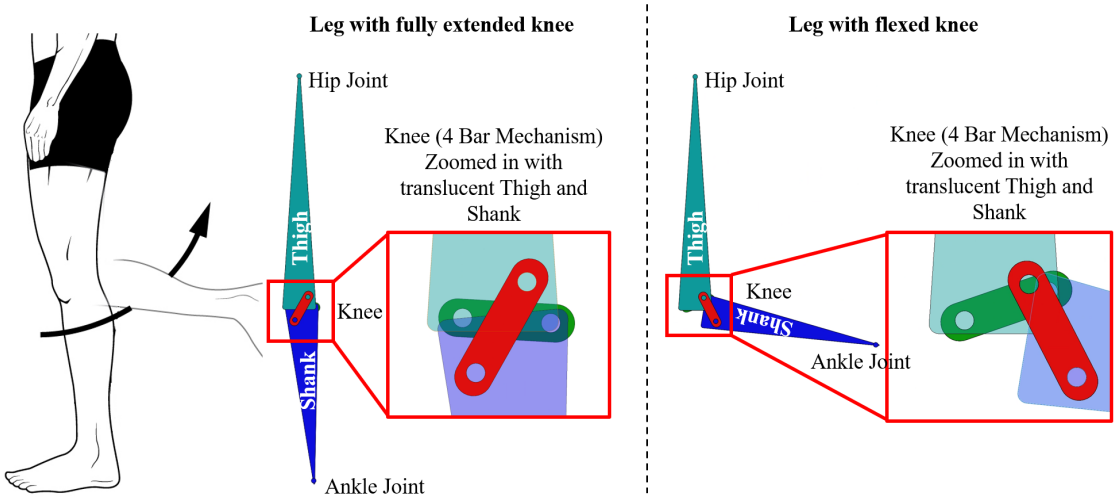

Figure 2.3: Model of the knee as a four-bar mechanism in the sagittal plane

3. CONTROL FRAMEWORK FOR WALKING WITH A TRANSFEMORAL PROSTHESIS ON LEVEL GROUND

The field of prosthesis design has been growing considerably over the past years, addressing the needs of both transtibial and transfemoral amputees [47, 48, 49]. Upon understanding the limitations of passive prostheses, researchers have made strides to develop powered prostheses [10, 11, 12, 13, 14, 15, 16, 17, 18, 19]. These prostheses implement control strategies that fall into two major groups: impedance controllers that attempt to mimic human joint impedance [13, 50] and feedback linearization with tracking controllers that follow optimized joint trajectories [51, 52, 53, 16]. Of the two classes, the former has displayed greater promise in mimicking human-like gait kinematics and kinetics. As stated in [13], an impedance controller enables the user to interact with the device and the surrounding much like in the case of healthy walking. An impedance controller consists of parameters pertaining to stiffness, damping, and the reference angles of the joints. By modulating these parameters, the joint torque required for support and propulsion of the human body can be generated.

According to [13], researchers sectioned the gait cycle into 4-6 phases based on kinematic changes observed in a healthy human gait cycle (refer Figure 2.1). This is known as the finite state machine. Each phase has a set of three constant values–stiffness, damping, and the reference angle. The control input at any instant t in the gait cycle is given by

$$\tau(t) = K(\theta(t) - \theta_{ref}) + D\dot{\theta}(t) \tag{3.1}$$

where K and D represent the joint stiffness and viscous damping respectively. The term θ_{ref} is the reference or equilibrium angle of the joint, while $\theta(\cdot)$ and $\dot{\theta}(\cdot)$ signify the joint's position and velocity.

In [13], the joint control parameters (K, D, and θ_{ref}) were initially estimated using a least squares optimization that reduced the error between the torque of the impedance controller and

human torque data [42]. During testing, these estimates were tuned. Though successful, this approach mandated the manual tuning of several parameters. [27] attempted solving this issue through machine learning, but the manner in which one produces a labeled dataset is debatable since crucial parameters like user comfort are yet to be quantified. The study [54] implemented a series elastic actuator to modulate the impedance of the ankle joint in a transtibial prosthesis. Assuming the ankle to be a spring-damper system, the study estimated the stiffness parameters using a least squares optimization approach. The study, [55], proposed an ankle-foot exoskeleton that aided stroke patients in combating foot-drops. The system was manipulated using an impedance controller that was auto-tuned using a simple running-average-based-algorithm.

Varying the parameters as a function of gait characteristics has the benefit of fewer states in the finite state machine and hence fewer tuning parameters. [50, 56] varied K and θ_{ref} as functions of the joint angle and vertical ground reaction force during mid and terminal stance. The parameters were held constant during all other states in the finite state machine. Yet, both these approaches involved tuning 12 parameters per joint. Additionally, the inclusion of a load cell increases the weight and cost of the device. A recent study by [57] suggested using a continuous reference angle in contrast to the discrete set of reference angles implemented in [13]. This study has raised questions regarding the effect of discrete reference angles on the performance of impedance controllers.

3.1 Hypothesis and objectives

Clearly, lowering the number of states in the finite state machine would reduce the number of tuning parameters. An objective of this dissertation is to design a control framework with fewer states in the finite state machine that can generate healthy gait kinematics and kinetics. This work draws inspiration from the prior works involving least-squares estimates. It is wished that the joint control parameters vary as a function of gait characteristics, but it is also desirable to avoid relying on load cells like [50]. Instead, this work hypothesizes that there exist relationships between the control law parameters and gait progression. To test this hypothesis, three objectives were determined. (i) Determine continuous functions relating the stiffness and damping parameters to gait progression. (ii) Study the impact of the number states in the finite state machine. (iii) Propose

a control framework wherein all parameters (i.e., stiffness, damping, and reference angle) vary as continuous functions of gait progression. The focus of the first two objectives will be the ankle joint. The third objective will include both the ankle and knee joint. Section 3.2 presents the first two objectives. The related work has been published in [1]. Section 3.3 presents the last objective.

3.2 Stiffness and damping functions, and the impact of the number of states in the finite state machine

This section addresses the prior listed Objective 1 and 2. The process of estimating the stiffness and damping functions is fundamentally similar to the one used by [13]. It is desired that the generated torque from Eq. 3.1 be similar to that found in healthy human walking [42], say τ_{data}. Thus, the optimization problem minimizes the error between the torque τ and τ_{data}. Per [59, 60, 61], healthy human ankle joint stiffness and damping parameters continuously vary throughout the gait cycle in a smooth manner. Most of the variation in these parameters is observed during the stance phase, while the parameters adopt an almost constant value during the swing phase. To permit the continuous variation of stiffness and damping, while maintaining minimal decision variables, the stiffness and damping parameters were represented by polynomials during the stance phase. The orders of the polynomials were adjusted to get a better fit (i.e., reduce the difference between τ and τ_{data}). During the swing phase, the control parameters were assigned constant values: k_{swing} and d_{swing}. Supposing m and n represent the order of the stiffness and damping polynomials, the control parameters at any instant during the gait cycle are determined as follows.

$$K(t) = \begin{cases} \sum_{i=0}^{m} k_i t^i & \text{for } 0 \leq t < 0.63 \\ k_{swing} & \text{for } 0.63 \leq t \leq 1 \end{cases} \tag{3.2}$$

$$D(t) = \begin{cases} \sum_{i=0}^{n} d_i t^i & \text{for } 0 \leq t < 0.63 \\ d_{swing} & \text{for } 0.63 \leq t \leq 1 \end{cases} \tag{3.3}$$

[1] N. Anil Kumar et al., IEEE ICRA, 2020 [58]

Note that $t = 0$ is equivalent to 0% of the gait cycle, while $t = 1$ signifies 100% of the gait cycle. In accordance with [42], it is assumed that swing phase occurs at 63% of the gait cycle. Per the requirement for continuity in the control parameters, $k_{swing} = k_0$ and $d_{swing} = d_0$. Much like [13], the gait is sectioned based on kinematic changes, making θ_{ref} a set of angles. The optimization problem can be summarized as follows.

$$\min_{\theta_{ref}, k_i, d_i} \quad \|\tau_{data} - \tau\|_2 \tag{3.4}$$

$$\text{Subject to:} \quad K(t) \geq 0 \qquad D(t) \geq 0 \tag{3.5}$$

$$K(0) = K(1) \qquad D(0) = D(1) \tag{3.6}$$

$$\text{Continuity at } K(\phi_{TO}) \text{ and } D(\phi_{TO}) \tag{3.7}$$

$$|\Delta\tau/\Delta t| \leq c \tag{3.8}$$

The constraints listed in (4.4) force the positivity of the control parameters. Further, (4.5) ensures that the parameters maintain continuity between gait cycles and at the stance-to-swing transition. The last constraint, (4.7), forces the resulting τ to be continuous using a Lipschitz constant, c. Additional bounds were added, as needed, to restrict the value of the reference angles. The optimization problem was solved using Matlab's *fmincon*.

Table 3.1: The four sets of reference angles that resulted from sectioning the gait are as follows.

Set label	**Sections of the gait cycle**			
Set A	0% - 13%	13% - 40%	40% - 63%	63% - 100%
Set B	0% - 40%		40% - 63%	63% - 100%
Set C	0% - 60%			63% - 100%
Set D	0% - 100%			

To study the impact of the number of the states in the finite state machine, four sets of reference

angles were established. The first set echoes the one found in [13]. The gait cycle is sectioned in accordance with the foot contact sequence during the stance phase. The first phase initiates at ϕ_{HS} (0%) and continues until ϕ_{FF} (≈13%), followed by the second phase that terminates at ϕ_{HO} (≈ 40%). The third phase is between ϕ_{HO} and ϕ_{TO} (≈63%). Unlike [13], the swing phase of the gait cycle is not sectioned. The remaining three sets of reference angles implement fewer sections of the gait cycle. Table 3.1 lists said sets. The sectioning proposed in *Set B* is similar to the one proposed by [59].

3.2.1 Joint parameter functions

The minimum order of the stiffness and damping polynomials required to lower the optimal cost was determined to be 4. This study fixed the order of the stiffness and damping polynomial to be the same. The optimal τ resulting from the optimization has been shown in Figure A.1. It was observed that the trend of the stiffness and damping parameters was not sensitive to the reference angles set. Figure 3.1 depicts the stiffness and damping parameters. The associated polynomial coefficients can be found in Table A.3.

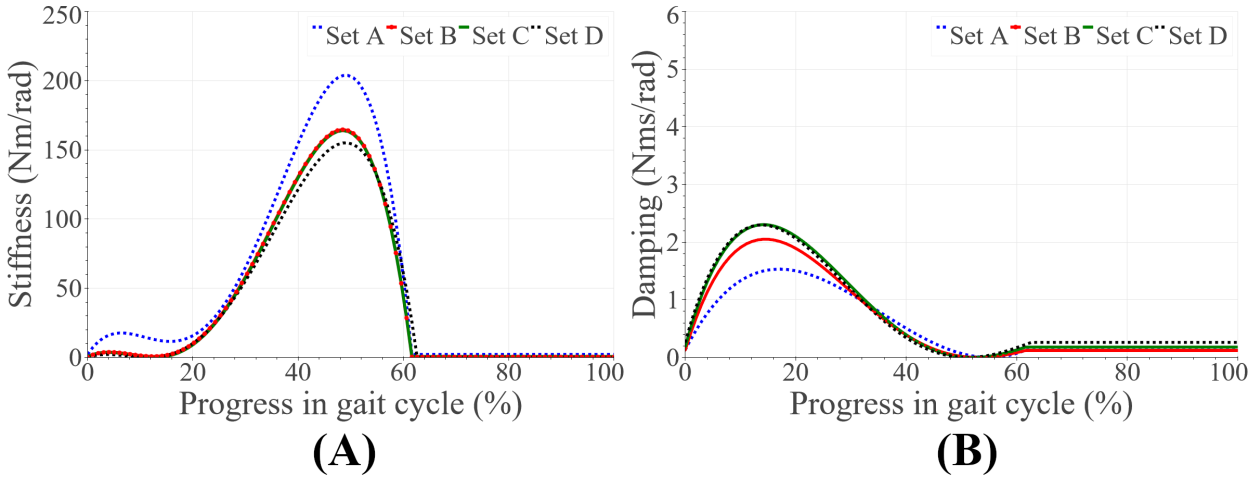

Figure 3.1: Optimization results. **Top**: Stiffness curves, **Bottom**: Damping curves..

Table 3.2 presents the reference angles that resulted from the optimization. *Sets A* to *C* showed

similarities by having the ankle plantarflexed during terminal-stance and dorsiflexed during swing. The plantarflexed angle helps store the potential energy needed for push-off. The dorsiflexed swing reference angle ensures foot clearance to avoid trips. The reference angle for *Set D* resembled a foot-drop condition–the state a human foot would conform to when physically unconstrained. It was anticipated that the foot-drop condition would pose a challenge during swing phase. It is likely that certain compensatory actions will be needed to ensure sufficient foot clearance during swing.

Table 3.2: Sets of multiple reference angles in radians resulting from the optimization

Set label	0% - 13%	13% - 40%	40% - 63%	63% - 100%
Set A	0.0294	-0.3428	-0.3491	0.3029
Set B	-0.4258		-0.4363	0.0000
Set C	-0.4363			0.1453
Set D	-0.4655			

3.2.2 Implementation

The proposed sets of control parameters were tested on a powered transfemoral prosthesis, AMPRO II, shown in Figure 3.2. While the proposed impedance controller was implemented at the ankle, a previously published controller–a hybrid of impedance and trajectory tracking–was used to manipulate the knee. The latter has been discussed in [62]. The following sections detail the hardware and the controller implementation.

3.2.2.1 Hardware

AMPRO II was operated by an embedded system (BeagleBone Black, element14, Leeds, United Kingdom) that controls an actuated ankle and knee joint. Said system runs at 200Hz. Each joint was equipped with Brushless DC (BLDC) motors (MOOG, BN28), (1:100) Harmonic drives (CSG-17-100-2UH-LW, Harmonic Drive), and (1:1.6) pulley-belt transmission. An optical rotary encoder (E5 Optical Kit Encoder, US Digital) was mounted at the end of the belt transmission.

Each motor was controlled using ELMO, G-SOLWHI motor drivers. The signals from the Beagle-Bone Black were relayed to the motor drivers using Controller Area Network (CAN) protocol. The prosthesis also had a passive spring-loaded toe joint. It was unclear whether the stiffness at AMPRO II's toe joint would impact the ankle's performance. To study the effect of each impedance controller, in an isolated manner, the toe joint was restrained using a rigid element. A force sensor (FlexiForce A502, Tekscan, South Boston, MA) placed under the heel helped detect heel-strike. This aided in determining the state in the finite state machine and the progress within each state.

3.2.2.2 Gait progress estimation

The prosthesis was operated under a time-based scheme that utilizes a parameter that linearly increases from 0 to 1 as the gait progresses from 0% to 100%. This parameter is used to identify the progress in the gait cycle. The force sensor placed under the heel was used to initialize the parameter.

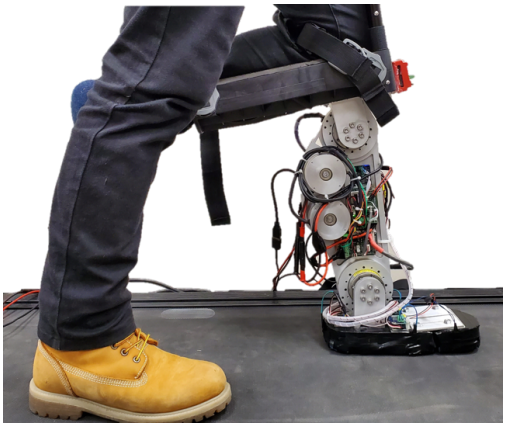

Figure 3.2: AMPRO II–a transfemoral prosthesis attached to a L-shaped emulator

3.2.2.3 Controller Tuning

The tuned reference angles have been documented in Table 3.3. In addition, the stiffness and damping curves were scaled down by factors α and β, respectively. This was done to limit the push-off assistance based on the participant's comfort and to abide by the motor's rated torque

specifications. A major drawback of scaling was that the stiffness during swing phase was no longer sufficient to transition from the plantarflexed reference angles during terminal-stance to the swing dorsiflexion angle. Thus, a constant stiffness term (γ) was uniformly added to the stiffness curve. The following equations describe the tuning process.

$$K_{tuned}(t) = \alpha K(t) + \gamma \tag{3.9}$$

$$D_{tuned}(t) = \beta D(t) \tag{3.10}$$

The scaling factors (α and β) were reduced until certain dorsiflexion was observed during the mid-stance phase. The term γ was increased until the ankle displayed dorsiflexion during the swing phase. Note that γ was not required for *Set D* since the reference angle remained constant throughout the gait cycle. The stiffness curve for *Set A* was scaled by a factor of $\alpha = 0.4$, while $\alpha = 0.5$ for the remaining sets. Further, while $\beta = 0.2$ for *Set A*, $\beta = 0.166$ for the remaining sets. The constant term γ was equal to 20 for all sets. These scaling factors will change based on the subject.

Table 3.3: The tuned sets of reference angles in radians

Set label	0% - 13%	13% - 40%	40% - 63%	63% - 100%
Set A	0.0100	-0.0875	-0.3490	0.0873
Set B	-0.1745		-0.2617	0.0000
Set C	-0.2617			0.1452
Set D	-0.2617			

3.2.3 Experiment

To validate the proposed idea, an indoor experiment was designed using the aforementioned powered prosthesis in Figure 3.2. A healthy young subject (male, 170cm, 70kg) participated in

the experiment using an L-shape simulator that helped emulate prosthetic walking. The subject was asked to walk on a treadmill at his preferred walking speed (0.7 m/s). The subject's safety was assured by handrails located on either side of the treadmill. The experiment protocol has been reviewed and approved by the Institutional Review Board (IRB) at Texas A&M University (IRB2015-0607F).

3.2.4 Results and Discussion

Figure 3.3 presents the average angular trajectory, torque, and power of the ankle for all four sets of control parameters. The averaged values represent 15-20 consecutive gait cycles. A Butterworth filter was used to process the data. The standard deviation was well-bounded, indicating the consistency of the observed results. Barring *Set D*, the trend of the kinematic and dynamic curves are similar across the control parameter sets. The trend also bears a resemblance to healthy human data reported in [42].

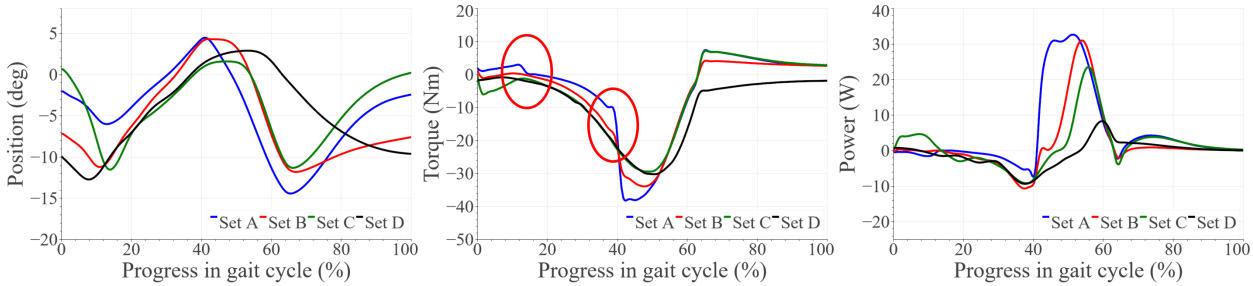

Figure 3.3: Averaged results of the experiments. **(A)** Ankle angle, **(B)** Ankle torque, and **(C)** Ankle power. The sections of the torque curve corresponding to foot-drop and heel-off have been enlarged.

3.2.4.1 Comparison of kinematics

It should be emphasized that the stiffness and damping curves portrayed similar trends across all sets of control parameters. Thus, the kinematics of the generated gait was dictated by the reference angles. The following observations form the basis of this claim: (i) *Set A* displayed lesser

plantarflexion proceeding heel-strike in comparison to the other sets owing to the dorsiflexed reference angles between heel-strike and foot-drop. *Set C* displayed foot slap (steep plantarflexion) proceeding heel-strike. Increasing damping could counter this issue. (ii) Lesser dorsiflexion was observed during terminal-stance in *Set C* and *D*. Unlike these sets, *Set A* and *B* increase the plantarflexed reference angle in increments. It is likely that such an incremental ascension assisted the subject in achieving higher dorsiflexion during mid- and terminal-stance (iii) The variance in ankle angles, among sets, at the beginning and end of the gait cycle is due to varying swing reference angles. It would be beneficial to implement a higher swing reference angle since it ensures sufficient foot clearance during swing (iv) Plantarflexion at push-off was greater in *Set A* due to the higher reference angle. Additionally, *Set A* showed an earlier descent from dorsiflexion to plantarflexion at heel-off (40%). A plausible explanation is that the combined effect of heightened stiffness and higher plantarflexion forced an earlier push-off (v) Evidently, *Set D* showed an absence of dorsiflexion during swing phase due to the plantarflexed reference angle. As anticipated, the foot-drop reference angle of *Set D* resulted in few stumbles during the swing phase [63].

A kinematic abnormality that cannot be overlooked is the absence of push-off in *Set D*. As stated earlier, the impedance control strategy was implemented using a time parameter that linearly increased as the gait progressed. With that said, the success of time-based control heavily depends on the subject's ability to synchronize his/her gait with the time parameter. This synchronization task proved to be a mighty challenge while testing *Set D*. Specifically, the constant foot-dropped reference angle introduced gait abnormalities such as exaggerated hip extension at toe-off. In preparation for the over-extended hip angle, the subject forcibly maintained a dorsiflexed ankle beyond peak stiffness (which occurs at 50% of the gait cycle). When toe-off eventually occurred, the stiffness was thus insufficient to quickly restore the ankle to the plantarflexed reference angles.

3.2.4.2 Comparison of dynamics

Set A and *B* resulted in higher torque during terminal-stance in comparison to the other sets. This is likely due to higher dorsiflexion in mid and terminal-stance (as discussed in Section 3.2.4.1). As a consequence, the corresponding power was higher in *Set A* and *B*. Most interesting to note

was the abrupt change in the torque corresponding to *Set A* at foot-drop (13%). Such a change was not observed in the results of the other sets. This is undoubtedly a consequence of the change in *Set A*'s reference angle at foot-drop. Similar behavior was observed at heel-off (40%) in the results of both *Set A* and *B*. Thus, fewer changes in reference angles ensure a smoother torque output. Further, the re-positioning of the ankle joint to the swing dorsiflexed angle resulted in positive torque at the beginning of the swing phase for *Sets A* to *C*. In regard to the power curves, *Set A*'s power output displays an aberrant increase at heel-off which is attributed to the high velocity at push-off detailed in Section 3.2.4.1. Finally, the push-off power associated with *Set D* was significantly lower due to the previously discussed delayed push-off.

3.2.5 Conclusion

The following results were revealed: (i) Multiple reference angles during the mid and terminal-stance phase that increase the plantarflexed reference angle in increments can assure more ankle dorsiflexion during mid-stance. Consequently, the generated torque and power at push-off are higher. (ii) Abrupt changes in torque can be expected at the instants when the reference angle switches. Such changes impact the robustness of the system to perturbations. This ideology is the motivation behind studies proposing a continuum of reference angles [57]. (iii) While overly plantarflexed reference angle during terminal-stance results in higher push-off torque, it can give rise to premature push-off. (iv) Most importantly, a single reference angle during stance phase is sufficient to generate human-like kinematics and dynamics at the cost of lower mid-stance dorsiflexion and foot slap at heel-strike.

3.3 Continuous joint parameters

It is believed that continuous parameters can help strike a balance between the necessity for fewer tuning parameters (achieved through lowering the number of states in the finite state machine) and the desired control over the generated walking kinematics and kinetics. The newly adopted control framework has the finite state machine shown in Figure 3.4. Unlike the earlier section, both the knee and ankle are now controlled. Here, a hybrid controller is adopted: impedance

control during stance and trajectory tracking during swing. The trajectory tracked during the swing phase is healthy walking joint trajectories ($\theta_{data}(t)$). The smooth transitioning between the two is facilitated by Bezier curves.

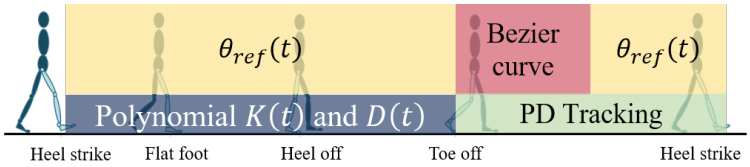

Figure 3.4: Finite state machine with continuous control parameters

This work recommends using polynomials for stiffness and damping but limiting them to stance. The reference angles also assume a polynomial during stance.

$$K(t) = \sum_{i=0}^{m} k_i t^i D(t) = \sum_{i=0}^{n} d_i t^i \theta_{ref}(t) = \sum_{i=0}^{n} \theta_i t^i \tag{3.11}$$

The process of determining these polynomial coefficients is similar to the one used in Section 3.2, but the nonlinear term $K(t)\theta_{ref}(t)$ must be decoupled to proceed. This work utilizes a heuristic for solving this problem which involves solving two optimization sub-problems iteratively until convergence. The two problems have been described below. The first solves for the stiffness and damping polynomial coefficients given $\theta_{ref}(t)$, while the second solves for $\theta_{ref}(t)$ given $K(t)$ and $D(t)$. Note that the estimation is limited to the stance phase since impedance control is used only during stance. However, it is desirable to have smooth transitioning between the reference trajectory in stance and swing. Thus, this work imposes constraints on the reference trajectory $\theta_{ref}(t)$ at the stance-to-swing transition and at the beginning of the gait cycle. Also implemented are suitable bounds on all parameters (lb and ub).

Sub-problem 1:

$$\min_{k_i,d_i} \quad \|\tau_{data} - \tau\|_2 \tag{3.12}$$

$$\text{s.t.} \quad lb \leq K(t), D(t) \leq ub \tag{3.13}$$

Sub-problem 2:

$$\min_{\theta_{ref_i}} \quad \|\tau_{data} - \tau\|_2 \tag{3.14}$$

$$\text{s.t.} \quad lb \leq \theta_{ref}(t) \leq ub \tag{3.15}$$

$$\theta_{ref}(0) = \theta_{data}(1) \tag{3.16}$$

$$\theta_{ref}(t) = \theta_{data}(t) \text{ at } t = \phi_{TO} \tag{3.17}$$

$$|\Delta\theta_{ref}(t)/\Delta t - \Delta\theta_{data}(t)/\Delta t| \leq c \text{ at } t = \phi_{TO} \tag{3.18}$$

Here, $\{\cdot\}_{data}$ corresponds to the healthy walking data from [45]. The constants lb and ub are listed in Table 3.4. The constant c was 0.0035 and the associated Δt was 1. The The initial guess for all polynomial coefficients was $[0\ 0\ 0\ 0\ 0]^T$. The problem was solved using Matlab's Scipy package. Unlike the earlier investigation, this optimization problem was solved for the ankle and knee. From iteration i to $i+1$ the difference in the solutions was calculated as follows:

$$e^{(i)} = \|\bar{k}^{(i)} - \bar{k}^{(i+1)}\|_2 + \|\bar{d}^{(i)} - \bar{d}^{(i+1)}\|_2 + \|\bar{\theta}^{(i)}_{ref} - \bar{\theta}^{(i+1)}_{ref}\|_2 \tag{3.19}$$

where $\bar{k}$, $\bar{d}$, $\bar{\theta}_{ref}$ are vectors containing the the stiffness, damping, and reference angle polynomial coefficients. The problem was said to converge when the cumulative $e^{(i)}$ over 5 consecutive iterations was less than 0.01. That is,

$$\sum_{i=0}^{4} e^{(i)} \leq 0.01 \tag{3.20}$$

Table 3.4: The bounds used in the optimization

	Ankle		**Knee**	
K (Nm/rad)	20.0	250.0	20.0	250.0
D (Nms/rad)	0.1	3.0	0.1	3.0
θ_{ref} (deg)	-12.0	12.0	0.0	40.0

3.3.1 Joint parameter functions

The optimization converged in 36 iterations for the ankle and 41 for the knee. The resulting control parameter functions have been depicted in Figure 3.5. The depiction of the plot $\theta_{ref}(t)$ (Figure 3.5 C) also includes swing trajectories. From the depiction, it was clear that the reference trajectory from stance smoothly transitions to the desired swing joint trajectories. The ankle stiffness curves resembled those in Section 3.2. Damping on the other hand was high at the beginning and end of stance. The reference angle also followed the trend assumed by the discrete θ_{ref} in Section 3.2. That is, mildly plantarflexed during initial and mid stance and severely plantarflexed during terminal stance. The knee, on the other hand, had higher stiffness during mid stance. The knee damping increased through the stance phase. Finally, the knee reference angle resembled healthy human walking trajectories. The polynomial coefficients for all control parameter functions have been tabulated in Table A.2. The associated tuned reference angles have been tabulated in Table 4.1.

3.3.2 Implementation

The proposed controller was tested on a powered transfemoral prosthesis, AMPRO II (shown in Figure 3.6(A)). The following subsections present details on the hardware, controller implementation, and the experiment with an amputee and an able-bodied subject.

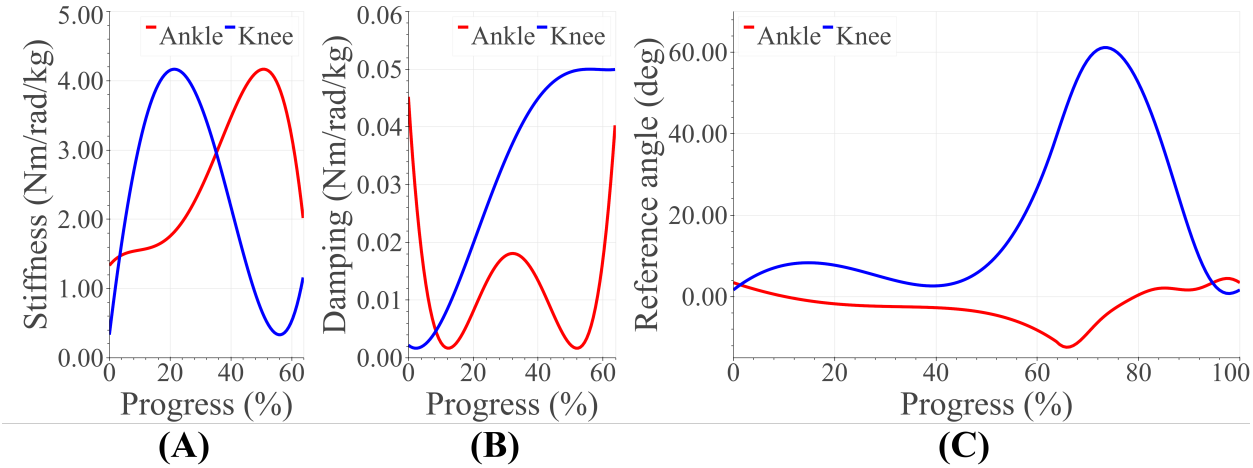

Figure 3.5: Optimization results: Control parameter functions of the knee and ankle

3.3.2.1 Hardware

This study also utilized AMPRO II (refer Section 3.2.2.1). Some modifications were however made. The prosthesis was now equipped with a 3D printed foot with a toe joint. A force sensor (FlexiForce A502, Tekscan, South Boston, MA) placed under the heel helped detect heel-strike, while an Inertial Measurement Unit (MPU 9150, SparkFun Electronics, Niwot, CO) affixed to the user's thigh measured the thigh angle. The latter's data was processed by a dedicated BeagleBone Black operating at 200Hz. The IMU data was filtered using a complementary filter. These two parameters helped determine the state in the finite state machine and the progress within each state.

3.3.2.2 Gait progress estimation

The progress in the gait cycle (t) is identified using a phase variable that monotonically increases from 0 to 1 as the gait progresses from 0% to 100%. The variable is initialized upon heel-strike detection. A phase portrait of the thigh angle against its integral over the course of gait cycle presents an ellipse. The arc-tangent of the two plotted parameters is among the most successful and popular candidates for a phase variable [64]. Normalizing factors determined in real-time from prior gait cycles, help manipulate the usual elliptical phase portrait into a more circular one.

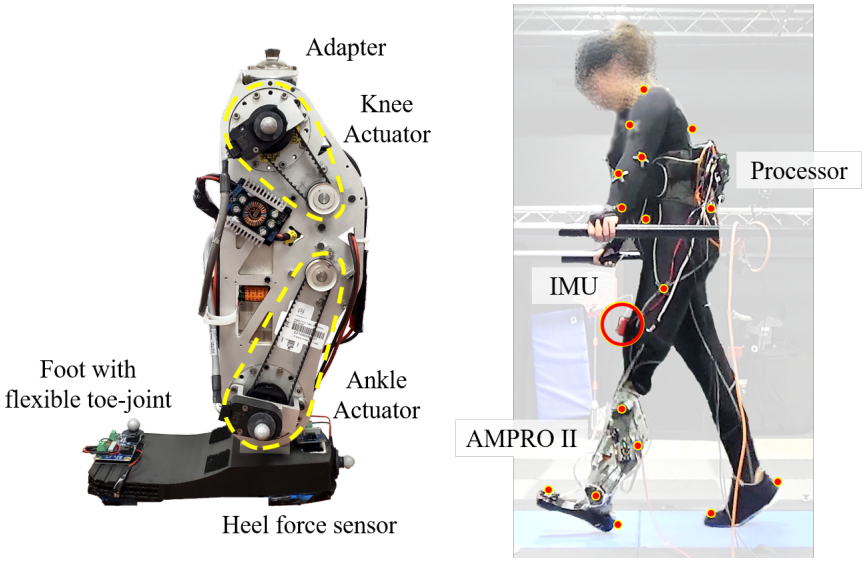

Figure 3.6: Experimental set up: **(A)** is the powered transfemoral prosthesis, AMPRO II, **(B)** shows the amputee walking with AMPRO II in a motion capture environment.

Doing so results in a more linearly varying phase variable and consistent state estimation [65].

3.3.3 Experiment

An indoor experiment was conducted with a transfemoral amputee (female, 164cm, 66kg w/o prosthesis). She utilizes a microprocessor knee, X3 Knee (Ottobock), with a Freedom Runaway Foot (Ottobock). The amputee was asked to walk with AMPRO II at 0.67 m/s. Eight training sessions with AMPRO II were conducted prior to data collection. All trials were conducted on an AMTI force-sensing tandem treadmill in a motion capture facility with using Vicon Vantage motion capture cameras. The experiment protocol has been approved by the Institutional Review Board (IRB) at Texas A&M University (IRB2015-0607F).

This work compared the proposed strategy (with continuous $K(t)$, $D(t)$, $\theta_{ref}(t)$) against one with continuous $K(t), D(t)$ and discrete reference trajectory. The former is called *continuous* and the latter is called *discrete*. The *discrete* strategy has 3 states during stance similar to that shown in Set A of Table 3.1. During swing, however, the strategy proposed in Figure 3.4 is used. The The associated polynomial coefficients can be found in Table A.3 (the coefficients of Comp1 and Comp2 must be linearly combined using scalars -0.0601 and 0.7977 respectively for the ankle,

and -0.6 and 1.315 respectively for the knee). These polynomial coefficients were determined using an optimization like the one in Section 3.2. More details can be found in Chapter 4.

3.3.4 Results and discussion

There were both kinematic and kinetic differences between *discrete* and *continuous* control schemes. Figure 3.7 presents the kinematic and kinetic results. The solid line represents the averaged data across 30 gait cycles, while the shaded region represents 1 standard deviation. Some kinematic and kinetic results have also been presented in Figure 3.8. The depicted results are dimensionless metrics attained through normalizing the measured values against the corresponding values from healthy walking data [42, 43]. Again, the depicted results correspond to the average across 30 gait cycles and the error bars represent 1 standard deviation.

On comparing the results of both schemes, the following observations were made. Compared to the *discrete* scheme, the *continuous* offered: (i) higher peak ankle dorsiflexion during mid stance, (ii) lower peak plantarflexion during terminal stance, (iii) lesser peak push-off torque and power, (iv) lower knee flexion and flexion torque during initial stance, (v) higher peak ground reaction force at initial stance and push-off. Interestingly, the standard deviation of some results corresponding to the *discrete* scheme was rather high. Namely, (i) peak plantarflexion, (ii) ankle torque at 40% of the gait cycle, (iii) push-off power, and (iv) peak ankle dorsiflexion during mid stance.

While higher push-off assistance is desirable, the higher push-off offered by the *discrete* scheme can be presumably inconsistent since the standard deviation is high. Further, the high standard deviation in ankle torque at 40% of the gait cycle agrees with the results documented in Section 3.2 wherein kinks (or discrete jumps) were observed in control input while transitioning between states of the finite state machine. Moreover, the higher ankle dorsiflexion and peak ground reaction forces with the *continuous* scheme is indicative of higher load transfer from the intact to the prosthesis. It is possible that the amputee trusted the device more, hence transferring more her weight onto the device. The ankle is also observed to dorsiflex earlier with the *continuous* scheme vs. the *discrete*. This earlier dorsiflexion is also observed in healthy walking and is perhaps the reason behind the higher load transference.

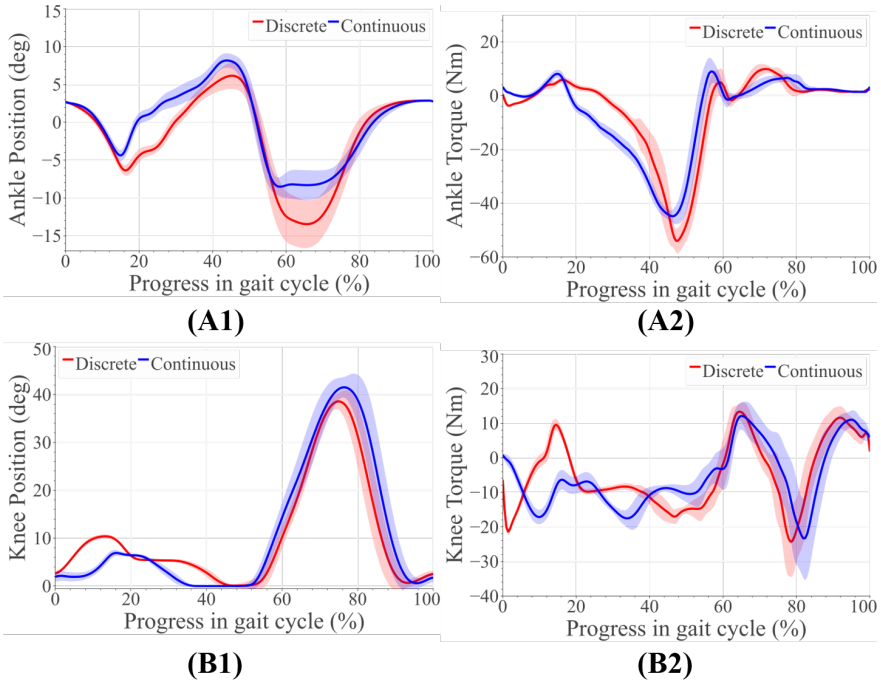

Figure 3.7: Experiment results comparing discrete and continuous reference trajectories.

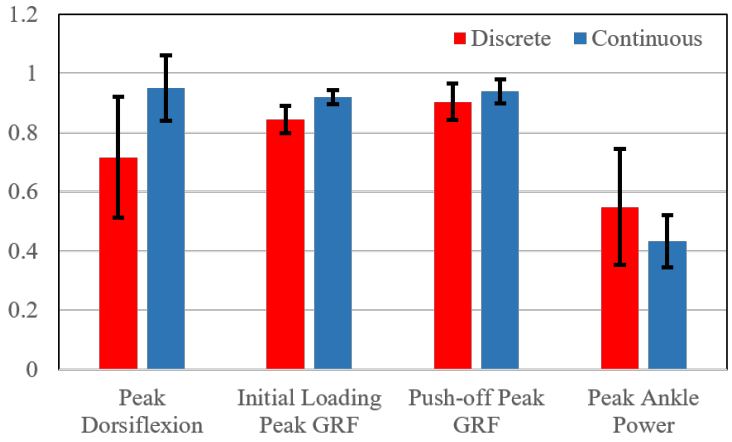

Figure 3.8: Peak ankle dorsiflexion, GRF, and power with discrete and continuous reference trajectories

The prior discussion raised questions about the consistency of walking kinematics with the *discrete* control strategy. To study this further, a phase portrait analysis was conducted. The 30 gait cycle trial was equally split into two trials which can now be treated as two trajectories with

different initial conditions. Figure 3.9 depicts the phase portrait of the resulting trajectories under both control schemes. The circular markers represent the instant of toe-off for each plotted gait cycle.

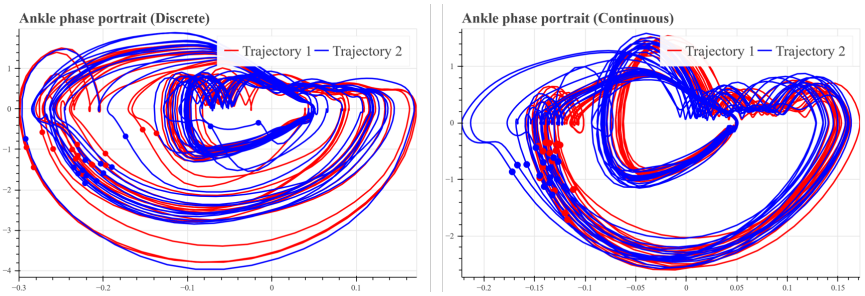

Figure 3.9: Phase portrait of the ankle joint with discrete and continuous reference trajectories

Studies such as [66] inferred the stability of walking by observing how clustered instants such as toe-off were in phase portraits. More closely clustered points were considered to signify more stable or consistent walking. Qualitatively, one could easily infer the existence of a limit cycle under the *continuous* scheme. However, such a conclusion is harder to draw from the phase portrait of the *discrete* scheme. This work utilized Kantz algorithm [67, 68] to quantify the rate of convergence to some limit cycle. This algorithm estimates the Lyapunov exponent by observing the evolution of the difference between two nearby points of interest (on two different trajectories) over several time steps. A more negative exponent represents faster rate of convergence. The points of interest, for this work, were the instants of toe-off. Each gait cycle was considered to be a time step.

The Lyapunov exponent for under the *discrete* scheme was found to be -0.0428, while the exponent under the *continuous* scheme was -0.1059. Given the higher magnitude of the latter, it may be inferred that the *continuous* scheme leads to more consistent walking and is more robust under perturbations. Studies such as [57] have postulated similar benefits of continuous reference trajectories. Specifically, they claim continuous reference trajectories would be more robust or

safer under inaccurate state estimation. The results of this work concur with the hypotheses laid out in [57].

3.3.5 Conclusion

This chapter proposed impedance control parameters that vary as continuous functions of the gait progress. Adopting said parameter functions significantly reduced the number of tuning parameters, thus easing user customization of level walking control strategies. Continuous control parameter function also lead to more consistent or stable walking, making them more reliable under uncertainties in state estimation. Finally, there were signs (e.g. higher load transference) that the amputee subject trusted the proposed framework more. This chapter thus strongly recommends further investigating continuous parameter functions.

3.4 Future work

The employed gait progress estimation scheme is known to perform poorly at lower walking speed [65]. This chapter strongly recommends solving this problem. Current estimation schemes only consider the thigh angle for in-gait progress estimation and utilize a heel mounted force sensor for gait cycle initiation. One avenue for improvement includes decomposing the estimation scheme into two: one for the stance phase and another for swing. A toe mounted force sensor can be used to detect the stance-to-swing transition. Such a scheme could prove more accurate under non-uniform walking speed and robust to perturbations while walking.

Finally, this chapter did not consider tuning the continuous reference trajectory. Tuning parameters such a scaling or offset factor could be considered in the future. That said, care must taken to maintain the continuity of the reference trajectory at heel-strike. Further, any modifications made to the reference trajectory must consider the nature of the real-time generated Bezier curve. For instance a severely plantarflexed angle at the end of stance can be further exacerbated by the Bezier curve, possibly leading to stumbles and falls.

4. CONTROL FRAMEWORK FOR WALKING WITH A TRANSFEMORAL PROSTHESIS ON SLOPED TERRAIN

In [13], the joint parameters were constant within each state in the finite state machine. Estimates for the parameters were determined through a least squares optimization that minimized the difference between the torque from Eq. 3.1 and the joint torque from healthy human walking data. While this approach has been proven to emulate healthy walking kinematics and kinetics, it involves careful tuning of the initially estimated joint parameters (numbering at 12-18 per joint). In [69], the authors recognized similarities between gait kinematics and kinetics on different slope angles, and suggested using the same impedance control strategy as in [13] but with different joint parameters. Despite its success, this process involved re-tuning the joint parameters for every slope angle.

Varying the parameters as a function of gait characteristics has the benefit of fewer states in the finite state machine and hence fewer tuning parameters. [50, 56] varied K and θ_{ref} as functions of the joint angle and the vertical ground reaction force during mid and terminal stance phases. The parameters were held constant during all other states in the finite state machine. While amputee trials proved the controller's success, the results in [50] were limited to level and upslope walking and [56] did not discuss gait kinetics. Furthermore, the controller's reliance on a load cell increases the ultimate cost and weight of the prosthesis. In [58], the joint parameters varied as a function of t during stance phase, thus no longer requiring a load cell. While the above approaches lessened the number of states during stance phase, [70] and [62] lessened the number of states during the swing phase by tracking healthy human walking trajectories. In fact, [62] exploited the similarities between the sloped walking knee swing trajectories by tracking the level walking trajectory regardless of the slope angle. The smooth transitioning between stance and swing phases was facilitated by Bezier curves and a low gain PD controller towards the end of the gait cycle helped with terrain adaptation. Despite having fewer tuning parameters, the application of the above approaches to sloped walking still requires re-tuning several parameters for every slope angle.

4.1 Hypotheses and objectives

The problem of re-tuning the joint parameters for every slope angle is worsened by the absent relationship between the joint parameters and the slope angle. The primary objective is to fill this gap in knowledge. The methods used in [58] and [62] form the foundation of this work. The objectives of the control framework for sloped walking were determined upon studying the kinematics and kinetics of sloped walking (refer to Chapter 2). Section 4.2, presents the control framework with estimates of the joint control parameters across all slope angles. The estimation is an extension of the one presented in [58] wherein K and D are polynomials of t. Upon estimating the joint control parameters for all slope angles, basis functions spanning the entire set were extracted and a mapping between the joint parameters and the slope angle was proposed. This mapping and the basis functions form the two contributions of this chapter. Section 4.3 discusses the implementation of the control framework on a powered transfemoral prosthesis. Also presented is a thorough tuning regime for the proposed control strategy. The experimental results with an amputee and an able-bodied subject are then reported and discussed in Section 4.5. Section 4.6 has the concluding remarks. A portion of following content has been published in [1].

4.2 Proposed Control framework

As stated in [70], it is beneficial to use impedance control during stance phase since the limb is in contact with the terrain. During swing phase, it suffices to merely track healthy human trajectories. Thus, this chapter proposes a finite state machine with 4 states for the ankle and 5 for the knee. Both joints have three states during stance phase with the switches at ϕ_{FF}, ϕ_{HO}, and ϕ_{TO}. In other words, State 1 begins at heel-strike and ends with ϕ_{FF}, followed by State 2 which concludes at ϕ_{HO}. State 3, the last state in the stance phase, ends at ϕ_{TO}. During these three states, the framework adopts the same strategy as in [58]. That is, K and D vary as polynomial functions of t, while θ_{ref} assumes constant values during each state.

During swing phase, ankle angle does not vary much regardless of the slope angle–a motion

[1] N. Anil Kumar et al., IEEE ICRA, 2021 [71]

achievable using constant K, D, and θ_{ref} values. The knee, on the contrary, is more animated, requiring a more motion rich trajectory. To achieve the desired motion while having few tuning parameters, the framework utilizes the strategy proposed in [62] to control the knee joint. That is, a single level-walking trajectory is tracked using a PD controller regardless of the slope angle. The level walking trajectory in [45] was used as the desired trajectory. A Bezier curve was generated in real-time to smoothly transition from the instantaneous position and velocity at ϕ_{TO} to a predefined point in the level-walking desired swing trajectory. Refer to Figure 4.1 for a pictorial representation of the control framework.

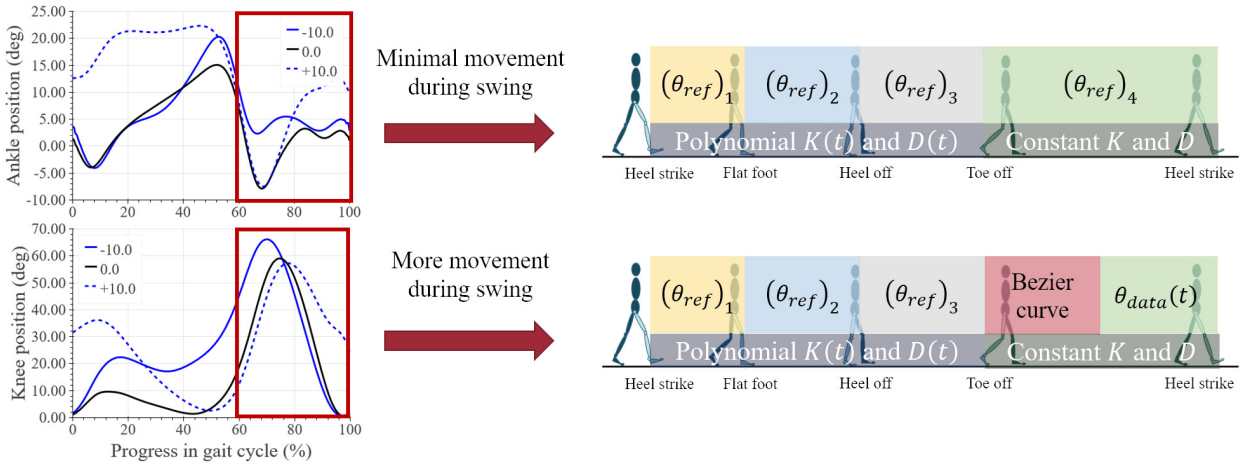

Figure 4.1: Control framework for sloped walking.

4.2.1 Estimation of joint parameter functions

To emulate healthy human gait kinetics using the impedance control strategy, joints parameters must be selected such that the torque produced is similar to that of healthy human walking, say τ_{data}. This chapter used the sloped walking data reported in [45] for τ_{data}, θ, and $\dot{\theta}$. The latter two are replaced by real-time angle and velocity feedback during implementation. An optimization that minimizes the norm of the difference between τ in (Eq. 3.1) and τ_{data} was formulated. Since the knee is controlled via impedance control only during stance phase, the knee's impedance

estimation (and thereby cost function) was limited to the stance phase.

Supposing m and n represent the order of the K and D polynomials respectively, the impedance parameters at instant $t \in [0,1]$ can be computed as follows,

$$K(t) = \begin{cases} \sum_{i=0}^{m} k_i t^i & \text{for } 0 \leq t < \phi_{TO} \\ k_0 & \text{for } \phi_{TO} \leq t \leq 1 \end{cases} \tag{4.1}$$

$$D(t) = \begin{cases} \sum_{i=0}^{n} d_i t^i & \text{for } 0 \leq t < \phi_{TO} \\ d_0 & \text{for } \phi_{TO} \leq t \leq 1 \end{cases} \tag{4.2}$$

The coefficients of the stiffness and damping polynomials are given by k_i and d_i respectively. The stiffness and damping parameters are assigned the values k_0 and d_0 during the swing phase. Doing so enforces continuity of the impedance parameters at heel-strike (i.e. $K(0) = K(1)$ and $D(0) = D(1)$). Presented below is the optimization problem:

$$\min_{\theta_{ref}, k_i, d_i} \quad \|\tau_{data} - \tau\|_2 \tag{4.3}$$

$$\text{Subject to:} \quad K(t) \geq 0 \qquad D(t) \geq 0 \tag{4.4}$$

$$\text{Continuity of } K \text{ and } D \text{ at } t = \phi_{TO} \tag{4.5}$$

$$|\theta_{ref}| \leq c_1 \tag{4.6}$$

$$|\Delta\tau / \Delta t| \leq c_2 \tag{4.7}$$

The decision variables are $\{\theta_{ref}, k_i, d_i\}$, where θ_{ref} is a set of reference angles, one for each state of the finite state machine. The constraints listed in Eq. 4.4 force K and D to be positive. The constraint (4.5) assures continuity of the joint parameter functions at toe-off. The scalar, c_1, is a bound on the reference angles. $c_1 = 16^\circ$ for the ankle and $c_1 = 36^\circ$ for the knee. Further, the constraint Eq. 4.7 forces the resulting τ to be Lipschitz continuous with constant c_2. Additional

bounds were added, as needed, to restrict the value of the damping parameters. The optimization problem was solved using Scipy's minimization function. Owing to the non-convex nature of the problem, a unique solution does not exist. Results from perturbation studies [60] and past studies using least squares approaches [69] helped judge the feasibility of the estimated joint parameter functions. Future efforts will involve solving the optimization problem using heuristics to decouple the stiffness and reference angles, and guarantee convergence.

4.2.2 Joint control parameter functions

For both the ankle and the knee, $m = n = 4$ achieved the best results. The resulting ankle control parameter functions obeyed some monotonic trends across slope angles: (A1) Ankle stiffness during State 1-2 (ϕ_{HS} to ϕ_{HO}) was higher on steeper downslope and upslope terrain. The higher stiffness aids in stability during load transference from the trailing limb to the leading limb. (A2) During State 3, ankle stiffness increased as downslope angle grew less steep and the upslopes angle grew more steep. Here, the higher stiffness helps store more potential energy, resulting in higher push-off work. (A3) Ankle damping was found to be higher in downslope walking during State 1-2. The higher damping helps counter the higher heel-strike impact. (A4) The ankle reference angle during State 1 and State 4 was close to 0° during level and downslope walking, while it was dorsiflexed to match the slope angle during upslope walking. (A5) In State 2-3, the ankle reference angle greatly influences the generated push-off work. The angle is mildly plantarflexed during State 2, followed by a higher plantarflexed angle in State 3. The steepness of the reference angles increased with the steepness of the slope angle. The values of the angles have been reported in Table 4.1.

The following points are some of the key trends observed in the knee joint parameter functions. (K1) The knee stiffness during State 1-2 was higher at steeper downslope angles, aiding again in countering heel-strike impact and load-transference. (K2) On upslope terrain, the knee stiffness obeyed an opposite trend during State 1-2. The decrease in knee stiffness with the steepness in the upslope angle is believed to enable the required higher knee flexion for terrain adaptation. (K3) During State 3, the knee stiffness is higher on steeper upslope angles allowing for more

Table 4.1: Ankle and knee reference angles that resulted from solving the optimization problem and post tuning. Values for the slope angles not included can be found through linear interpolation.

	From optimization				**Post tuning**			
	Ankle Reference Angles (deg)							
Slope	State 1	State 2	State 3	State 4	State 1	State 2	State 3	State 4
-10.0°	-0.03	-3.94	-5.56	3.58	0.00	2.50	-5.00	0.00
-5.0°	-2.45	-5.30	-14.59	2.75	0.00	0.50	-7.50	0.00
0°	5.60	-11.06	-16.00	0.84	0.00	-2.00	-10.00	2.00
$+5^\circ$	4.82	-14.78	-16.00	0.75	4.00	-2.00	-10.00	4.00
$+10.0^\circ$	7.19	-15.0	-16.00	6.37	8.00	-2.00	-10.00	8.00
	Knee Reference Angles (deg)							
Slope	State 1	State 2	State 3		State 1	State 2	State 3	
-10.0°	8.90	10.36	30.00		11.97	10.26	16.33	
-5.0°	13.32	14.21	26.00		11.12	8.04	13.86	
0°	10.26	5.83	13.86		10.26	8.00	13.86	
$+5.0^\circ$	23.52	15.80	20.17		11.12	8.04	13.85	
$+10.0^\circ$	36.00	24.61	20.00		11.97	10.26	13.85	

propulsive knee extension while climbing up. (K4) Knee damping was found to be high during State 2 at steeper slopes (upslope or downslope), while remaining relatively the same during less steep slopes. (K4) The knee reference angles were more flexed on steeper slopes (downslope and upslope).

Basis functions spanning all stiffness and damping functions for each joint were extracted using Principal Component Analysis. The functions and their weights have been shown in Figure 4.2. The weights of the basis functions were found to vary monotonically within downslope and upslope walking. Some aberrations were observed, namely: (i) the ankle stiffness weights were higher than anticipated during downslope walking, leading to a discontinuity in weights from downslope to level walking. (ii) the ankle damping weights during downslope walking did not portray strong monotonicity. (ii) the weights corresponding to the knee's functions at -2.5° did not abide by the

monotonic trends. These observations are attributed to the anomalies in the data set (discussed in Section 2.2.2). These peculiarities are accounted for during controller implementation and tuning. The corrective measures are reported in the sections that follow.

4.3 Implementation

The proposed controller was tested on a powered transfemoral prosthesis, AMPRO II (shown in Figure 3.6(A)). The hardware and controller implementation is the same as that implemented in Section 3.3.

4.3.1 Controller tuning

Given the slope's angle, an initial guess for joint stiffness and damping can be found using the impedance basis functions and their weights. The resulting stiffness and damping functions can be tuned further to generate the desired gait kinematics and kinetics. Prior to tuning, both joint parameter functions should be multiplied by the subject's body mass. This chapter proposes tuning the joint parameter functions as follows.

$$K_{tuned}(t) = \alpha K(t) + \gamma \tag{4.8}$$

$$D_{tuned}(t) = \beta D(t) \tag{4.9}$$

where α and β are scaling factors, and γ is an offset. Each joint has its own scaling and offset terms. Enumerated below is the tuning procedure. This chapter recommends tuning the controller for level, -10°, and $+10^{\circ}$ slope, followed by linearly interpolating parameters for other slope angles.

1. The factor α affects the amount of resistance provided by the system to ankle dorsiflexion and knee flexion. With the ankle, lowering α reduces push-off assistance, while with the knee, lowering α challenges the stability of a flexed knee. Perform the following in iterations.

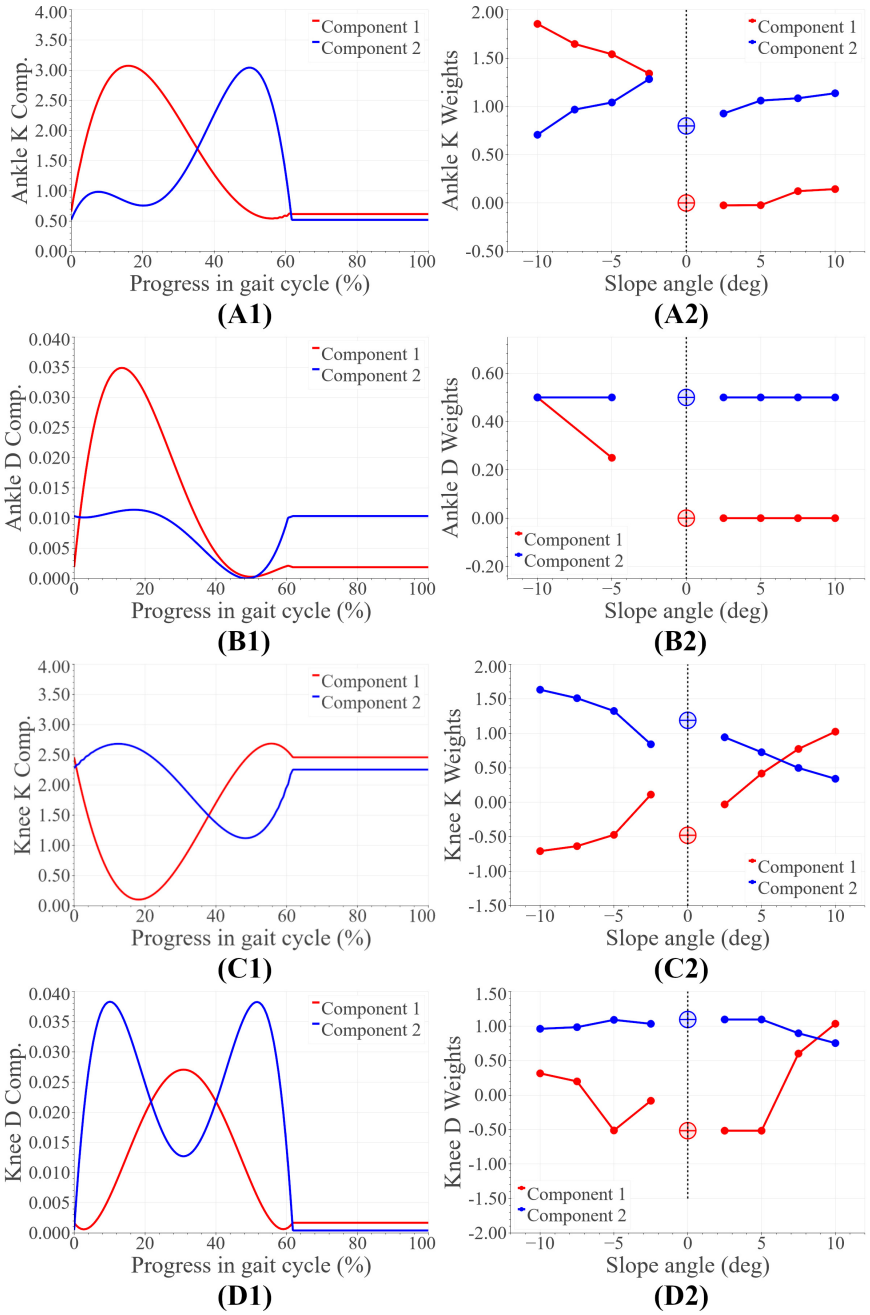

Figure 4.2: Basis joint parameter functions: **(A1)** and **(B1)** represent the ankle stiffness (Nm/rad/kg) and damping (Nm/rad/kg) basis functions, while **(A2)** and **(B2)** are the corresponding weights. **(C1)** and **(D1)** represent the knee stiffness (Nm/rad/kg) and damping (Nms/rad/kg) basis functions, while **(C2)** and **(D2)** are the corresponding weights.

(a) Decrease α until the desired ankle dorsiflexion and knee flexion is observed in State 2.

This chapter targeted 5° of ankle dorsiflexion and 10° of knee flexion.

(b) According to the participant's preference, increase or decrease push-off assistance by respectively increasing or decreasing the ankle's plantarflexed reference angle during State 3.

2. Tune β to reach a compromise between the amount of damping preferred by the participant at heel-strike and smooth terrain adaptation post heel-strike.

3. Increase the offset γ to counter gravity and maintain ankle dorsiflexion during swing phase and knee flexion during terminal stance phase.

4. For downslope walking:

   (a) set the ankle's swing reference angle to 0°.

   (b) reduce the knee's reference angles to within the acceleration limits of the actuators while maintaining more flexion than level walking. The reference angle during State 2 ensures smooth transition from State 1 to State 3.

5. For upslope walking:

   (a) increase ankle dorsiflexion and knee flexion in State 1 to facilitate terrain adaptation while respecting the actuators' acceleration limits.

   (b) set the ankle's swing reference angle to be equal to that in State 1.

   (c) reduce the knee's reference angle during State 2 to be lower than that in State 1. Accordingly reduce State 3 reference angle to obey the actuators' acceleration limits.

6. Tune the ankle's State 2 reference angle to allow easy transitioning from State 1 to State 3.

4.4 Experiment

An indoor experiment was conducted with a transfemoral amputee (female, 164cm, 66kg w/o prosthesis). She utilizes a microprocessor knee, X3 Knee (Ottobock), with a Freedom Runaway Foot (Ottobock). The amputee found walking on slopes uncomfortable even with the accustomed

microprocessor prosthesis. Thus the amputee was only asked to walk at slopes angles -5°, $+5^\circ$ with both AMPRO II and her microprocessor knee. The amputee underwent 8 training sessions with AMPRO II before data collection. To demonstrate feasibility of the controller on steeper slopes, a healthy young subject (female, 164cm, 50kg) was asked to walk with the prosthesis used an L-shape simulator. The healthy subject walked at -10°, -5°, 0°, $+5^\circ$, and $+10^\circ$. All trials were conducted on an AMTI force-sensing tandem treadmill in a motion capture facility with using Vicon Vantage motion capture cameras. The amputee chose to walk at 0.54m/s on slopes, while the able-bodied subject walked at 0.62m/s. A low speed was selected to avoid fatigue and assure safety. The chosen walking speed was fixed across all slope conditions. The controller was also tested with the amputee at 0.72m/s on level ground to demonstrate the feasibility of the proposed controller at different walking speeds. The safety of the participant was assured with handrails located on either side of the treadmill. Figure 4.3 depicts the amputee walking on different slopes, while Figure 4.4 pertains to the emulator chapter. Figure shows the able-bodied subject walking on different sloped terrain. The experiment protocol has been approved by the Institutional Review Board (IRB) at Texas A&M University (IRB2015-0607F).

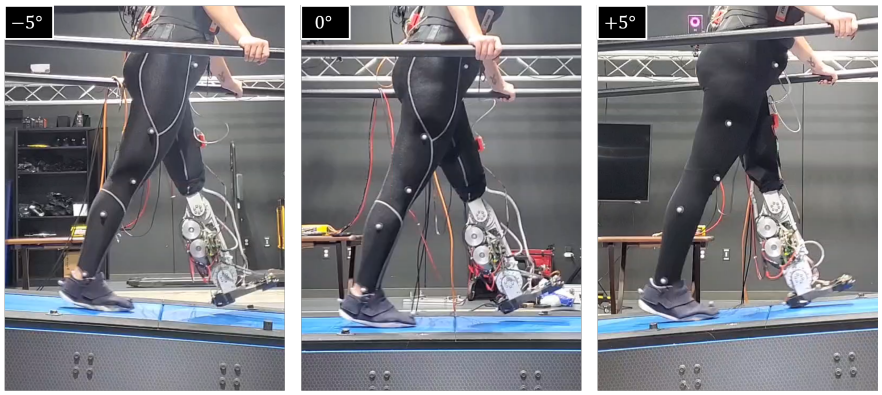

Figure 4.3: Amputee walking on sloped terrain with AMPRO II.

To assess the amputee's gait dynamics with the microprocessor knee markers were places on the lower body bony landmarks. Vicon Nexus was used to capture, filter, and interpolate marker

data. Visual 3D software was then used to create a model specific to the user and calculate angles and torques.

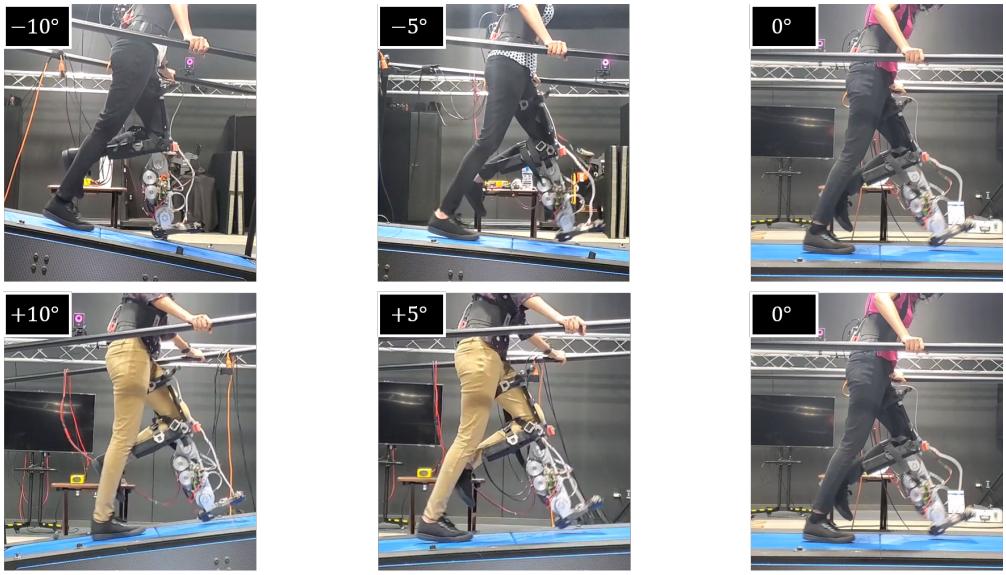

Figure 4.4: Able-bodied subject walking on sloped terrain with AMPRO II.

4.5 Results and discussion

For both amputee and able-bodied subject, the ankle's and knee's tuning parameters were as follows. $\alpha = 1$, $\beta = 1$, and $\gamma = 50$ for level and upslope walking. During downslope walking, $\alpha = 0.67$. This value is consistent with the observations in Section 2.2.1, i.e. the downslope walking kinematic data in [45] is higher than the expected value by a factor of $1.5 = 1/\alpha$. The tuned reference angles can be found in Table 4.1. The final proposed scheme in Section 4.6 accounts for this corrective factor. The results for the amputee and able-bodied subject have been presented in Figure 4.6 and Figure 4.7 respectively. The gathered kinematics and kinetics were filtered using a Butterworth filter with a cut-off frequency of 20 Hz. The results correspond to the average of 10 gait cycles. Figure 4.8 reports the peak ankle push-off for both subjects.

4.5.1 Amputee trials

Figure 4.5 presents the amputee's walking data with AMPRO II at two speeds. As the walking speed increased, Note an increase in ankle dorsiflexion during terminal stance phase and ankle plantarflexion during toe-off.

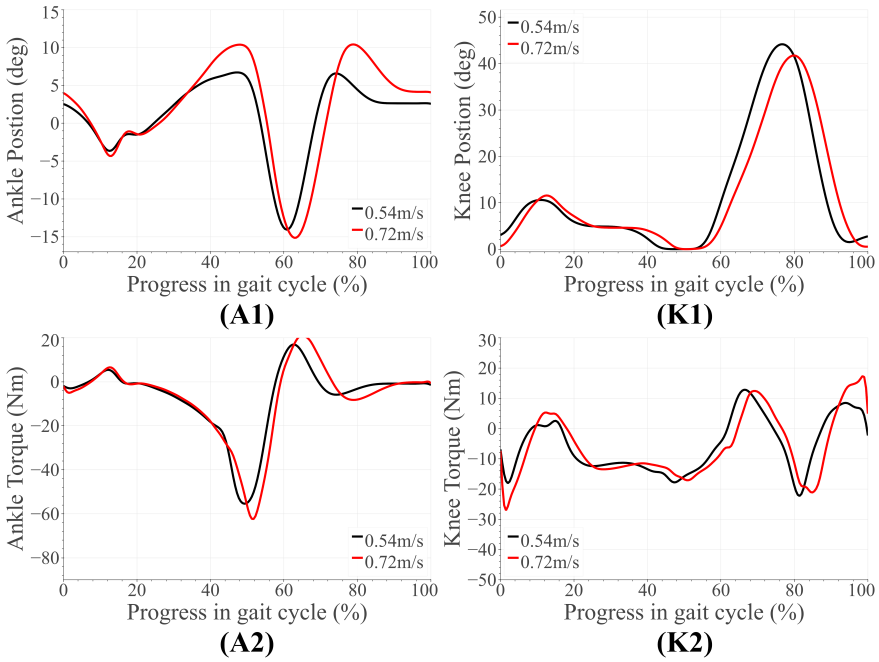

Figure 4.5: Amputee results for level walking with AMPRO II at different speeds. The subfigures labelled **(A1)** and **(A2)** correspond to the ankle, while those labelled **(K1)** and **(K2)** are for the knee.

The amputee's gait with both AMPRO II and the microprocessor knee on slopes (Figure 4.6) portrayed some trends similar to those found in healthy walking (see Section **??**). The ankle push-off moment, amount of knee extension moment between 40-60% of the gait cycle, and peak ankle push-off power increased as the slope varied from downslope to upslope. Also observed was higher ankle dorsiflexion at the beginning and end of the gait cycle during upslope walking. During downslope walking, the amputee's microprocessor knee was heavily flexed during stance phase, resulting in high flexion knee moment.

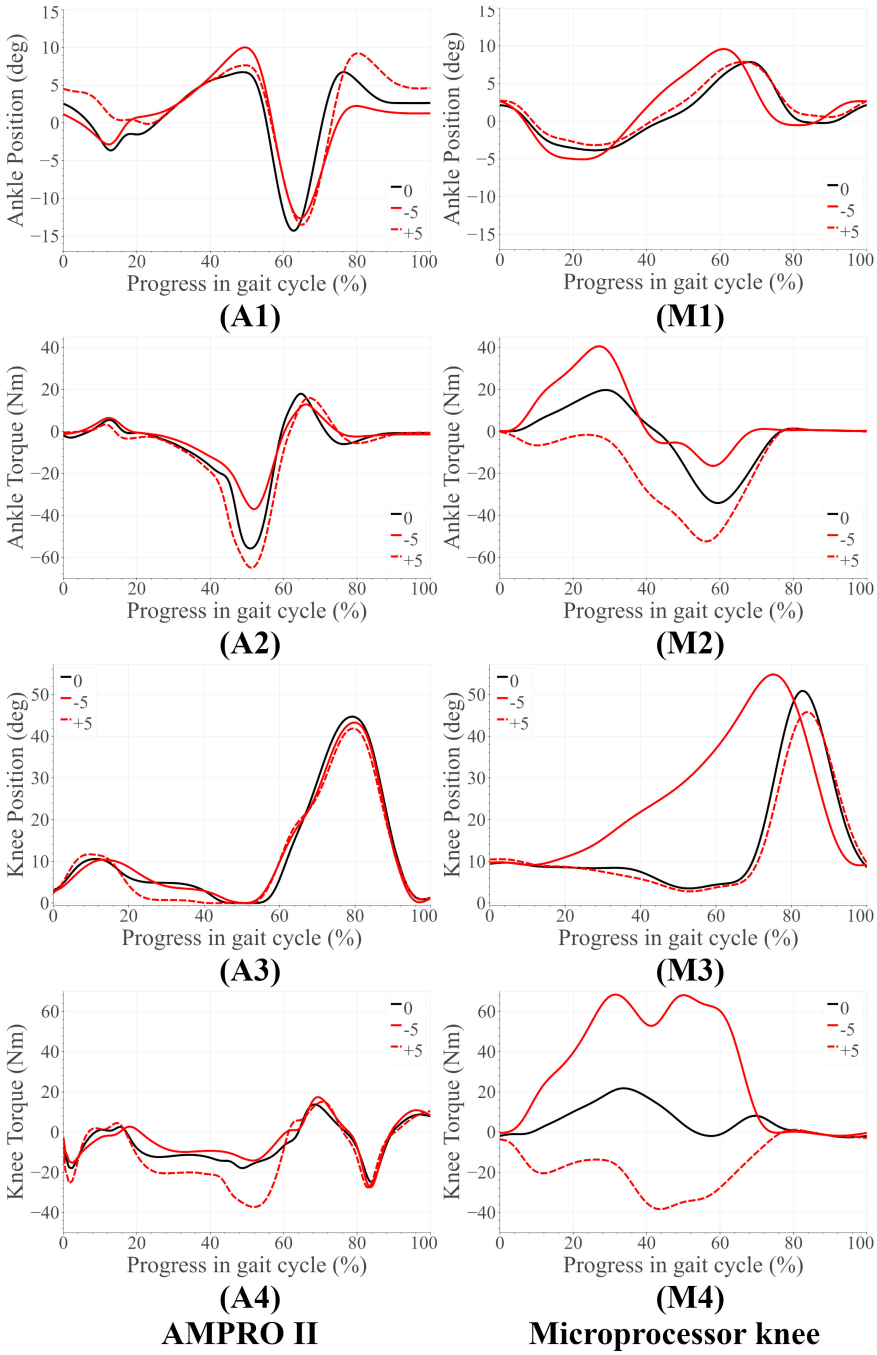

Figure 4.6: Amputee results for upslope walking and downslope walking. The subfigures labelled **(A)** correspond to the AMPRO II ankle joint, **(M)** are for the Microprocessor knee prosthesis

The amputee was able to walk with AMPRO II at various walking speeds. The push-off assistance and the kinematic differences noted earlier have been well documented in able-bodied walking studies [43, 45]. This proves the feasibility of the control scheme at different walking

speeds. While using AMPRO II, the amputee's sloped walking kinematics and kinetics obeyed the monotonic trends found in healthy walking. With more gait training, these results are expected to improve. While using her microprocessor knee, knee flexion gradually increased from heel-strike to approximately 70% of the gait cycle (Figure 4.6M3). This gradual yielding is due to the passive nature of the device, i.e. the device offers no active resistance to knee flexion. Studies such as [72] have made similar observations with other microprocessor knees. Additionally, the higher ankle dorsiflexion at the beginning and end of the gait cycle while walking upslope implies terrain adaptation. These results prove the feasibility of the control scheme for amputees.

4.5.2 Able-bodied trials

Some notable trends observed in ankle kinematics include: (i) higher dorsiflexed ankle at the beginning and end of the gait cycle on upslopes with the dorsiflexion increasing as the steepness of the slope increased, (ii) lesser toe-off plantarflexion on downslopes, (iii) higher knee flexion during initial stance phase on sloped terrain than level ground. In terms of kinetics, it was observed: (i) that the ankle peak torque and power (Figure 4.8) varied monotonically with the angle as it varied from -10° to $+10^\circ$, (ii) higher knee extension torque on upslopes.

The variation in ankle angle at the beginning and end of the gait cycle facilitates terrain adaptation. The higher plantarflexion at toe-off during upslope walking is correlated to the higher push-off torque and power. Higher push-off assistance is required as the slope varies -10° to $+10^\circ$. The higher extension torque, ankle push-off torque and power on upsloped terrain are all correlated with this need for higher push-off assistance. All of these trends are observed in healthy walking (detailed in Chapter 2), proving the feasibility of the control scheme on steeper slopes.

4.6 Conclusion

Proposed here is a sloped walking control framework with fewer states in the finite state machine than the state-of-the-art controllers. The framework includes impedance control during stance phase and trajectory tracking during swing phase. The smooth transition between the two is facilitated by Bezier curves. The joint control parameters were determined through a data-driven

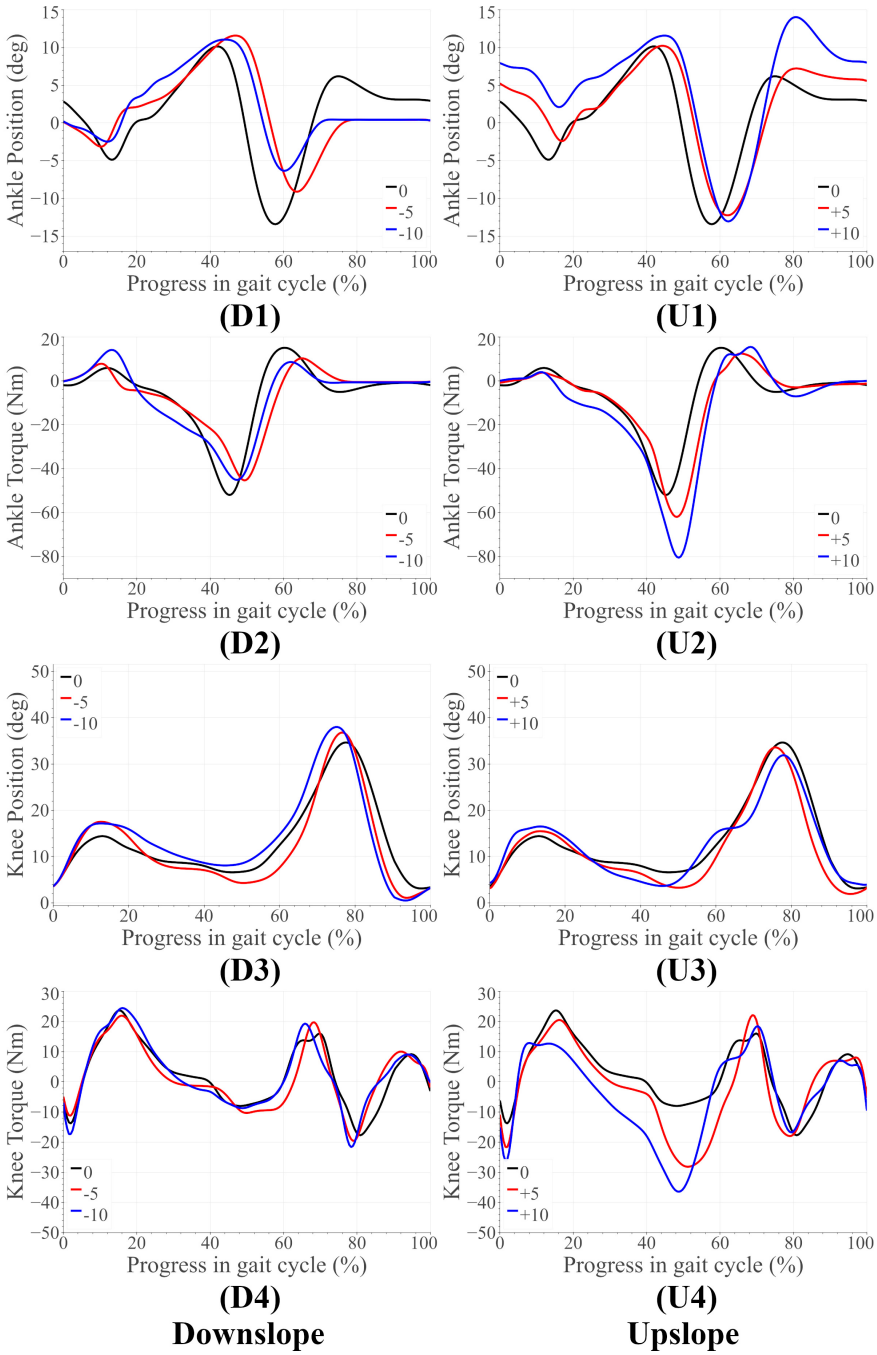

Figure 4.7: Able-bodied subject results for upslope walking and downslope walking. The subfigures labelled **(U)** correspond to the upslope walking, while those labelled **(D)** are for downslope walking.

optimization. Basis functions spanning the entire set of joint parameter functions were found through Principle Component Analysis. Given any slope angle, the stiffness and damping control

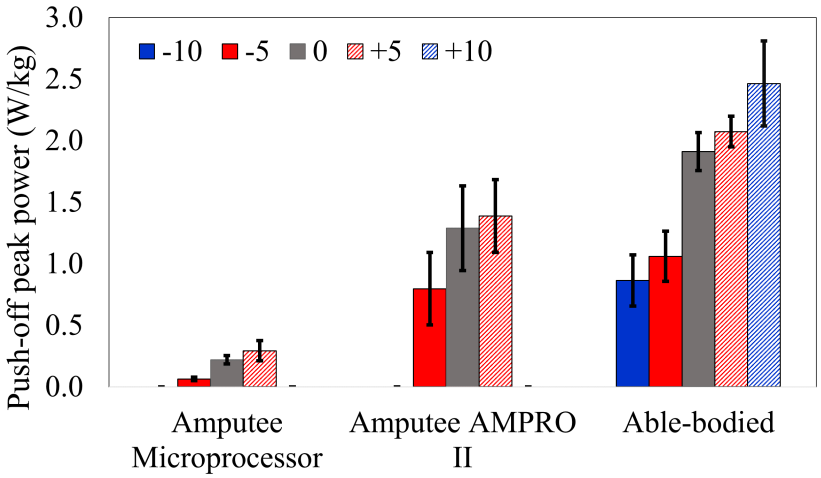

Figure 4.8: Peak ankle push-off power experience by the amputee with the microprocessor knee and AMPRO II. Also shown in the peak push-off power experienced by the able bodied subject with AMPRO II.

parameters can be found as follows:

$$K_{tuned}(t) = \alpha(w_{K1}(\psi)K_{Comp1}(t) + w_{K2}(\psi)K_{Comp2}(t)) + \gamma \tag{4.10}$$

$$D_{tuned}(t) = \beta(w_{D1}(\psi)D_{Comp1}(t) + w_{D2}(\psi)D_{Comp2}(t)) \tag{4.11}$$

where K_{Comp1}, K_{Comp2} represent stiffness basis functions, while D_{Comp1}, D_{Comp2} are the damping basis functions. The associated polynomial coefficients can be found in Table A.3. The weights for these basis polynomials vary as functions of the slope angle and are represented by $w_{K1}(\psi)$, $w_{K2}(\psi), w_{D1}(\psi)$ and $w_{D2}(\psi)$. The coefficients of the weights have been tabulated in Table 4.2.

A thorough tuning routine has also been prescribed in this chapter. The tuning process can be automated using rule-based fuzzy logic. Testing with an amputee and able-bodied subject proved the feasibility of the proposed scheme at varying slope angles. Monotonic trends consistent with healthy human walking data were observed in both kinematics and kinetics. To name a few: push-off assistance (from both ankle and knee joint) increased as the slope angle increased from downslope angles to upslope angles, and the ankle angle at the beginning and end of the gait cycle varied

according to the slope angle–enabling terrain adaptation.

Table 4.2: Weight functions for the ankle and knee joint control parameter basis functions

	Ankle	**Knee**
$w_{K1}(\psi)$	$-0.137\psi - 0.060$ for $\psi < 0$, 0 otherwise	$0.005\psi^2 + 0.090\psi - 0.270$
$w_{K2}(\psi)$	$0.032\psi + 0.84$	$-0.001\psi^2 - 0.065\psi + 1.106$
$w_{D1}(\psi)$	-0.05ψ for $\psi < 0$, 0 otherwise	$0.001\psi^3 + 0.014\psi^2 - 0.002\psi - 0.621$
$w_{D2}(\psi)$	0.5	$-0.003\psi^2 - 0.007\psi + 1.118$

4.7 Future work

Future work involves improving the phase variable based estimation scheme for sloped walking. Currently, phase variable schemes do not account the relationship between toe-off timing and slope angle (i.e. toe-off timing is delayed as the slope varies from steep downslope to steep upslope terrain). Improving the scheme would greatly reduce the standard deviations of peak push-off power seen in Figure 4.8. A possible approach is to mount a force sensor at the toe and update the toe-off timing–in the finite state machine–from one gait cycle to another. Another improvement to the existing control scheme involves employing a continuously varying reference angle. Doing so would improve the stability of the system under uncertainties in state estimation [57]. Additionally, a continuously varying reference angle could further reduce the number of states in the finite state machine, further easing user customization of the proposed control scheme.

5. SELF-ALIGNING POLYCENTRIC MECHANISM FOR KNEE ORTHOSES

The human knee is a complex mechanism with a center of rotation that constantly changes throughout the gait cycle. When limited to the sagittal plane, the knee is known to both rotate and slide [46, 38]. At any given instant, the center of rotation is referred to as the Instantaneous Center of Rotation (ICR). The locus of the ICR is termed centrode. Clearly, a pin joint knee exoskeleton will naturally misalign with the rotational axis of the human knee. This misalignment leads to device migration (i.e. the device moving from the initially affixed position) and higher interaction forces that eventually lead to skin sores, pain or injuries [25, 26]. Interaction forces are strongly correlated with the safety and comfort of lower limb orthotics/exoskeletons [73, 74, 75]. Despite this, researchers proceed to utilize single axis mechanisms in their exoskeletons/orthotics [20, 21, 22, 23] owing to its simplicity. The study [76] attempted to solve this issue by employing linear slides at the cuffs of the orthosis. These slides allow an initial adjustment of the device's center of rotation during fitment. Once aligned, the slides are arrested, imposing a single center of rotation. While this approach allows for customizing the device's center of rotation, it would still lead to misalignment while performing activities. There is thus a need for polycentric mechanisms.

Conventional polycentric knee mechanisms are of two types: (i) Polycentric mechanism with a Predefined Centrode (PPC), (ii) Polycentric mechanism with a Self-aligning Center of rotation (PSC). PPC solutions involve mating components that roll and translate much like the human knee. Some typical designs are: (i) meshed spur gears with a third link connecting the centers of the gears [77], (ii) cam-like mechanisms [34, 78, 79]. The former is preferred in actuated mechanisms for better transmission efficiency. Both designs have a predefined centrode which is either designed to suit a diverse group of users [34] or customized to the user [35]. Studies such as [34, 78, 79] determined an optimal centrode given knee kinematic data of a few subjects. While the optimized centrode represented a common best fit to the selected population, discrepancies are to be expected when dealing with a larger user base. The study [35] noted this issue and proposed custom designed centrodes for the user. Though such customized joints will perform better than

conventional designs, the development process can be highly demanding.

Researchers thus support using self-aligning mechanisms. These mechanisms follow one of the two approaches: (i) introduce linear allowances in the knee mechanism to enable self-alignment [39, 80, 41] or (ii) implement redundant actuators to control both rotation and translation of the joint [81]. The latter requires estimating the user's ICR and then suitably aligning the device's ICR. Currently there are no effective methods of estimating a user's ICR in real-time. Furthermore, both approaches to self-aligning mechanisms result in complicated designs that are hard to fabricate. Proposed herein is a simple, yet novel, knee mechanism that facilitates self-alignment. The design approach is similar to [81] in that allowances are introduced. Moreover, none of the proposed self-aligning mechanisms have been compared against conventional SA and PPC designs. This lack of comparative data is perhaps why PSA designs are not widely used today.

5.1 Limitations of current knee orthosis

As stated earlier, conventional knee orthoses implement a simple pin joint mechanism. Figure. 5.1 depicts the bare features of a knee orthosis affixed to the human knee model from Figure. 2.3. This dissertation limits the analysis to the knee's movement in the sagittal plane. The left sub-figure establishes the following notation: (Part 1) is the upper belt that is strapped around the user's thigh, (Part 2) represents a link that is rigidly connected to Part 1 and links Part 1 to a pin joint motor, (Part 3) is the link that is rotated by the motor, and (Part 4) is the lower belt that is attached to the user's shank. Note that Part 3 is rigidly attached to Part 4. This sub-figure also presents a side view that depicts the orthosis acting in parallel to the human knee.

The lengths of Part 2 and Part 3 have been arbitrarily chosen to be 100 mm. Further, no attempt was made to align the rotational axes of the knee and the motor. If the two belts were rigidly attached to the human limbs, it is quite apparent that the knee would not be able to flex owing to the axes mismatch. The right sub-figure of Figure. 5.1 demonstrates the knee flexing if the lower belt was allowed to slide along the shank. This sliding motion is indicated by the distance 53.06 mm reducing to 23.44 mm (a movement of 29.62 mm). This sliding motion is termed device migration and is believed to induce high interaction forces. To counter the misalignment, a

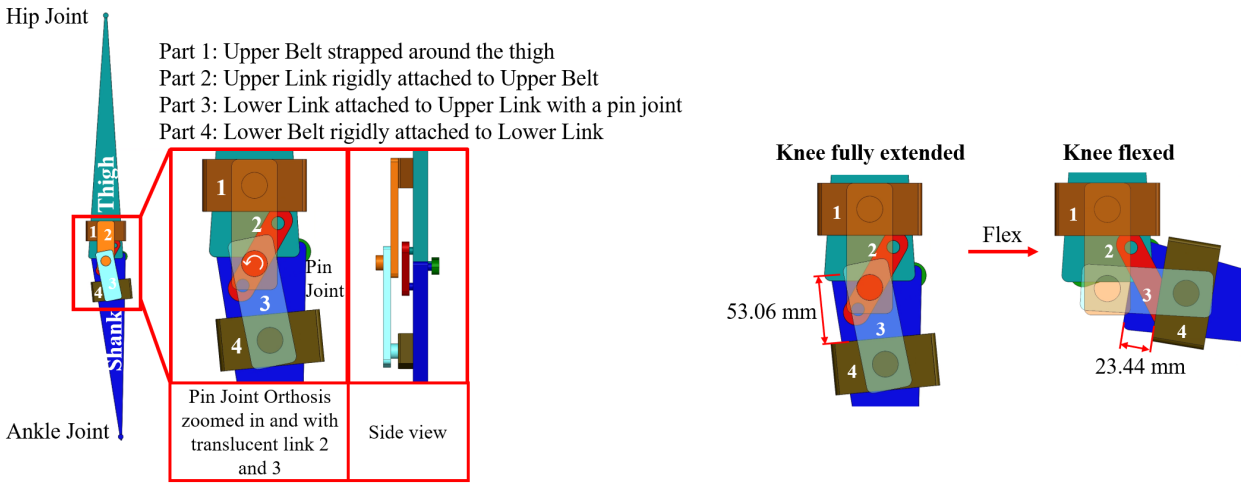

Figure 5.1: Left: A conventional pin joint knee orthosis acting in parallel to the human leg. Right: Knee flexed with conventional orthosis

considerable amount of time would have to be spent while donning the exoskeleton and trying to rid the axis mismatch. This chapter discusses a novel method to reducing axis misalignment and device migration. In turn, it is hoped that the time required to don the exoskeleton will also reduce. The following section presents the hypothesis and objectives of this chapter.

5.2 Hypothesis and objectives

The working hypothesis is that introducing allowances at the cuffs of knee mechanisms will reduce both device migration and interaction forces. This hypothesis will be proved by comparing a design with allowances to the state-of-the art. Section 5.3 presents the proposed design and alternative designs. Section 5.4 reports the method of comparing the proposed design against the state-of-the-art. The comparison involved a $n = 10$ human subject trial with 3 different knee mechanisms. The results of the comparison are presented and discussed in Section 5.5. The final section consists of the concluding remarks.

5.3 Proposed self-aligning knee orthosis

As a thought experiment, the rigid constraint between Part 3 and Part 4 was lifted. Instead a cylindrical allowance of 5mm was introduced. This allowed the contact point between Part 3 and

Part 4 to slide around within a circle. The left sub-figure of Figure. 5.2 depicts the cylindrical allowance. Upon including the allowance, the knee was able to flex by 10.13° while the lower

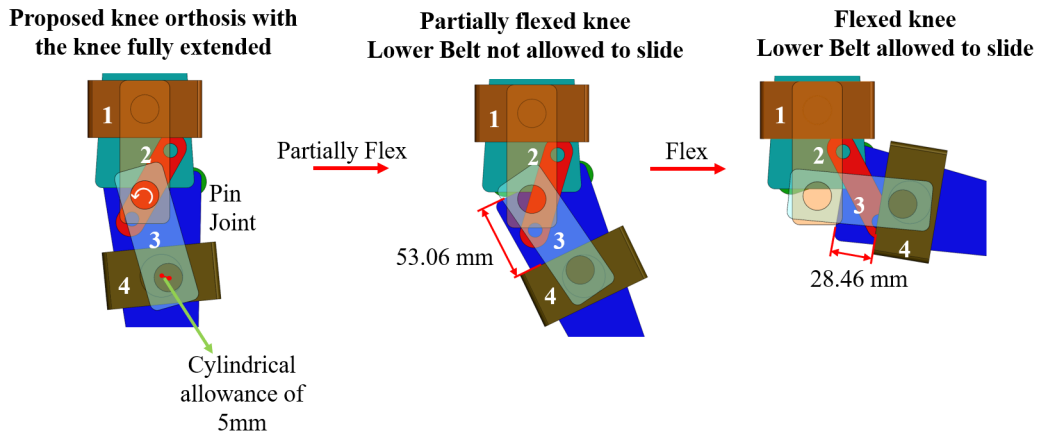

Figure 5.2: Left: Proposed knee orthosis design with a cylindrical allowance. Middle: Partially flexed knee. Right: Fully flexed knee

belt was rigidly attached to the shank. The middle figure in Figure. 5.2 depicts the partially flexed state. To completely flex the knee, the belt was allowed to slide along the shank. But as seen on the right of Figure. 5.2, the belt only moved by 24.6 mm. This demonstration verified the feasibility of reducing device migration by introducing an allowances at the cuffs. To further improve the range of motion from the partially flexed state of 10.13° (i.e. with the belts rigidly attached to the human limbs), a linear allowance of 5 mm was introduced between Part 1 and Part 2. As a result the knee flexion (while the belts were rigidly affixed) increased to 19.61°. Finally, the length of Part 2 and Part 3 was increased 160 mm. The results of these parametric changes have been listed in Table. 5.1.

5.4 Experiment: Comparison against state-of-the-art

The purpose of this section is to compare the proposed mechanism against the conventional knee mechanisms. Overall, three mechanisms were compared: (i) Single axis (SA), (ii) Polycentric joint with a Predefined Centrode, and (iii) Polycentric joint with a Self-aligning Center of rotation

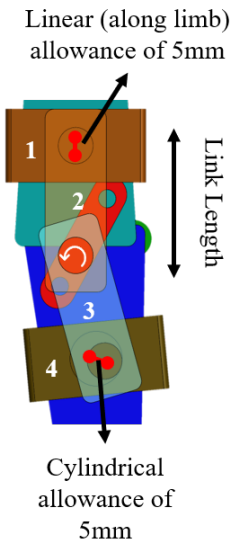

Figure 5.3: Design parameters of orthosis

Table 5.1: Knee flexion resulting from parameter changes. The inclusion of parameter is represented using a check or cross mark

Link Length (mm)	Cylindrical allowance	Linear allowance	Knee flexion (°)
100	✓	✗	10.13
100	✓	✓	19.61
160	✓	✗	21.74
160	✓	✓	34.03

(PSC). The latter is the proposed design.

5.4.1 Hardware

Figure 5.4 depicts all mechanisms. A Control brace consisting of no constraining mechanism was also tested. The chosen PPC brace had meshed spur gears and the PSC brace is an approximation of the proposed design from the prior section. Several steps were taken to limit the experiment's variables to only the mechanism designs listed above. Each knee mechanism was affixed within a compression knee brace [77]. Doing so standardized the brace's material, weight, inherent compliance (or stretch), and brace-strap design across the comparison.

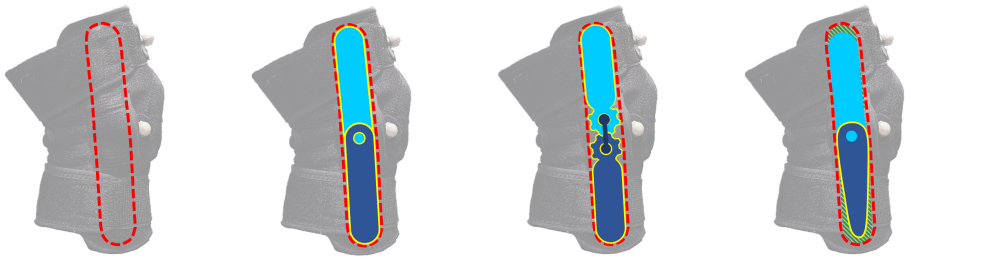

Figure 5.4: Knee brace mechanisms

The loads imposed by the brace's straps were measured using flexible force sensors (shown in Figure 5.5). These sensors were mounted along the sides of the limbs because: (i) interaction forces are expected to be maximum at the straps, (ii) the strap's sides are always in contact with the subject's limbs through the knee's range of motion. On the other hand, the front of the thigh strap, for instance, comes apart from the limb when the knee is flexed. This creates a gap between the brace and the limb, making this region not ideal for interaction force measurement. All braces with constraining mechanisms were fitted to within ± 1.0 N of each other. Doing so, maintained the fit across all mechanisms.

The Control and first constraining brace were fitted to the subject's comfort. Note that the Control brace was not considered while determining the desired forces at both straps. Since the Control brace did not have a constraining mechanism, the forces measured was always lower than the remaining three braces. Once fitted, the forces at the bottom and top sensor were recorded as f^0_{bottom} and f^0_{top} respectively. The sensor readings were collected and transmitted using a wireless processing unit consisting of an Arduino Micro and XBee Pro wireless module. The unit was placed in a vest worn around the subject's torso. The receiver unit consisted of a XBee Pro wireless module and an Arduino Uno, which transmitted the received data to a computer for storing. Figure 5.6 presents the setup pictorially. The loop rate of the receiving unit was 90Hz. The package utilized for the Xbee was Arduino's SoftwareSerial. The data transmitted to the computer was

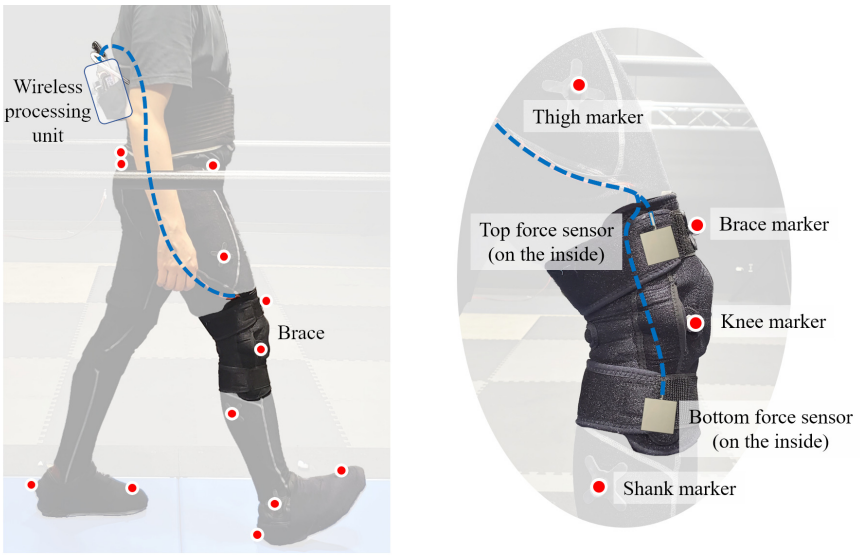

Figure 5.5: Experiment Setup: **(A)** subject with markers and a brace, **(B)** markers and sensors mounted on the brace

accessed using Python's Serial library. Said data was stored to a CSV file.

5.4.2 Protocol

With all participants, the Control brace was tested first and was tightened to the user's comfort. The position of the brace was determined as follows: (i) the brace was first fitted to comfort and the position was marked using masking tape, (ii) the subject was then asked to walk at a self-selected

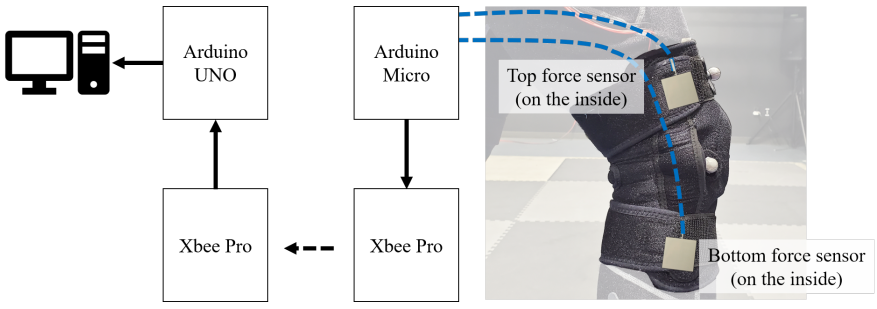

Figure 5.6: Architecture of the force sensor collection unit

pace for five minutes, (iii) the brace migration (if any) was measured (with respect to the initial fitment point, refer Figure 5.7) after five minutes. If the brace migrated from the initial position by more than 1 cm, the brace was refitted and the process repeated. Otherwise, the position was marked and fixed across all other braces. The process was repeated three times. If the subject failed all three times, the participant was ruled an outlier and the experiment concluded. In total, 10 participants (age 28±2.5 years, mass 70.5±11.2 kg, height 171.3±5 cm, 7 male and 3 female) successfully completed the experiment. Subject details can be found in Appendix Table A.4. After the brace was fitted, markers were placed on lower limb bony landmarks and the brace's hinge.

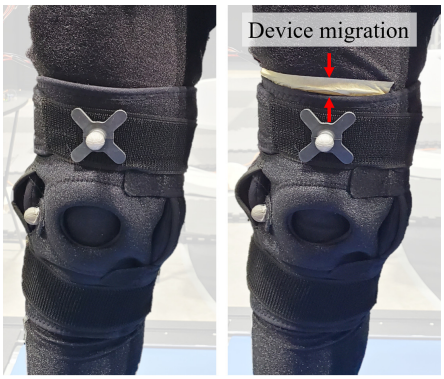

Figure 5.7: Device Migration, **(A)** the brace at the beginning of the trial, **(B)** the brace at the end of the trial with the white tape marking the reference for measuring device migration.

Motion capture data (Vantage Vicon Cameras) was collected over each trial consisting of: 20 leg raises, followed by 7 minutes of walking at 1.23 m/s speed, and concluded with another 20 leg raises. Refer to Figure A.3 for a pictorial representation of the trial. Two metrics were used to compare the knee mechanisms: (i) device migration–the distance between the top of the brace and the masking tape–, (ii) peak interaction forces at the top and bottom strap measured by the flexible

force sensors across the trial. The device migration, M_i, for each constrained brace was defined as

$$M_i = \frac{m_i - m_{Control}}{m_{Control}} \tag{5.1}$$

where m_i is the raw (un-normalized) migration for each constrained brace (i =SA, PPC, PSC) and $m_{Control}$ is the migration with the Control brace.

The force values were first filtered using a Butterworth low pass filter with a cut-off frequency of 10 Hz, after which the maximum value was determined. The filter used belonged to Scipy's signal processing library. Let f^*_{bottom} and f^*_{top} be the maximum force values at the bottom and top sensor, respectively. These values were then normalized for each constrained brace as follows.

$$F^*_{bottom} = \frac{f^*_{bottom} - f^0_{bottom}}{f^0_{bottom}} \tag{5.2}$$

F^*_{top} was calculated in a similar manner.

All metrics were checked for normality using the Shapiro–Wilk test ($\alpha = 0.05$, *scipy*'s *stats* library for Python). One-way repeated measures ANOVA was used to find the effect of the knee mechanism on device migration ($\alpha = 0.05$, the *statsmodels* library for Python). Post hoc tests used Fisher's least significant difference.

It is desirable for the range of interaction forces to be low and it is hypothesized that the interaction forces is positively correlated to device migration. The experiment has been approved by the Institutional Review Board at Texas A&M University (IRB2018-0837D).

5.5 Results and discussion

The normalized device migration and interaction force values have been shown in Figure 5.8. The ticks represent 1 standard deviation. The symbol * signifies $p < 0.05$ and ** implies $p < 0.005$. The Shapiro Wilk test revealed the normality hypothesis cannot be dismissed for migration data (SA: $p = 0.325$, PPC: $p = 0.109$, PSC: $p = 0.176$), top force sensor readings (SA: $p = 0.055$, PPC: $p = 0.205$, PSC: $p = 0.262$), and bottom force sensor readings (SA: $p = 0.135$, PPC:

$p = 0.188$, PSC: $p = 0.331$). The one-way repeated measures ANOVA revealed that the type of mechanism significantly affects device migration ($p = 0.0043$), top force sensor readings ($p = 0.007$), and bottom force sensor readings ($p = 0.0029$). The SA and PPC brace had significantly more migration than the PSC brace with $p = 0.022$ and $p = 0.007$ respectively.

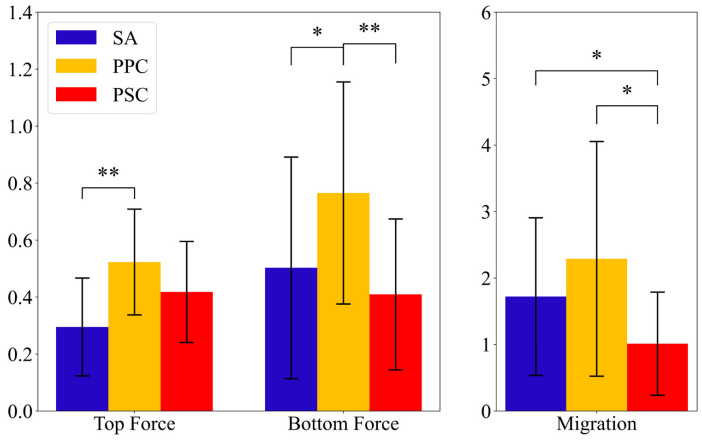

Figure 5.8: Average interaction force at top and bottom force sensors, and average device migration results

Although the device migration with SA was lower than that of PPC, the difference was not significant. The interaction forces on the top of the PPC brace was found to be significantly greater than SA brace ($p = 0.004$). The interaction forces on the bottom strap for the PPC brace was found to be significantly greater than both the SA ($p = 0.016$) and PSC braces ($p = 0.005$).

The PSC mechanism had significantly lower device migration than both SA and PPC, proving the benefits of self-aligning mechanisms. It also registered lower interaction forces than PPC at both the top and bottom force sensors, with the one at the bottom being significantly different. On the other hand, the interaction forces with PSC were not significantly different from those of SA. It is believed that the force readings pertaining to PSC were an overestimate. The design of the PSC mechanism is such that it moves within the brace's sleeve, which can incur additional

shearing forces. It is thus likely that the actual interaction forces with PSC are lower than the ones observed in this study. The working hypothesis is that the interaction forces and device migration are correlated, and that the PSC would out perform both SA and PPC per both metrics. Future work includes designing braces wherein the mechanism is placed away from the force sensors.

5.6 Conclusion

This chapter proposed a novel self-aligning knee mechanism and compared its performance against conventional designs. The three mechanisms compared were: (i) Single axis (SA), (ii) Polycentric joint with a Predefined Centrode (PPC), and (iii) Polycentric joint with a Self-aligning Center of rotation (PSC). The PSC mechanism saw the least migration out of all the mechanisms. Although it did not have significantly different interaction forces from the SA mechanism, this requires further investigation. The forces with PSC were however significantly less than the PPC brace on the bottom strap. The significantly lesser migration of the PSC brace shows that it can assist in reducing axis mismatch between the mechanism and knee. This provides evidence supporting the use of PSC mechanisms in orthotics and exoskeletons.

5.7 Future work

This chapter proposes testing rigid versions of the proposed self-aligning mechanism. A preliminary design of such a design can be found in Figure 5.9. The design consists of a spring loaded linear allowance at the thigh cuff and a spring loaded bi-directional allowance at the shank cuff. All allowances have linear bearings. The recommended spring stiffness is 2.582 N/m. This value was selected based on the peak interaction forces observed in the human subject trial. The selected stiffness is such that it offers minimal resistance against correcting the misalignment between the device and human knee joint. Yet, the stiffness value is high enough to counter the gravitational forces acting on the mechanism. A bill of materials for this design can be found in Table A.5.

As stated earlier, the design of the proposed brace design only consider the human knee's polycentric motion constrained to the sagittal plane. 3D mechanisms form another avenue for future research. Few studies have attempted this. Additionally, the design analysis only considered

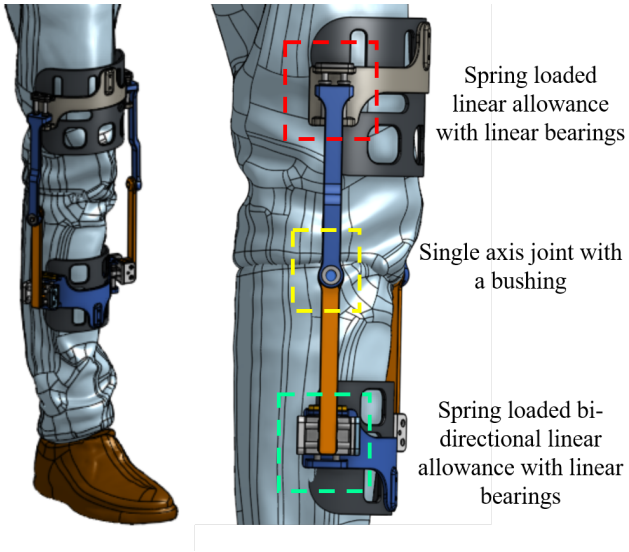

Figure 5.9: A knee orthosis employing the proposed self-aligning joint design

a healthy human knee. Injured knees could have severe translation, leading to a much longer centrode. Currently, the allotted 5mm of allowance at each cuff might be insufficient for an injured knee. This work recommends designing custom polycentric PPC mechanisms for such knees.

6. SUMMARY AND FUTURE WORK

User customization of lower limb assistive devices remains a challenge in the field of rehabilitation. It mandated changes to both the mechanical and control system of the device. This dissertation outlined three problems: two related to the control of transfemoral (above knee) powered prostheses and a third regarding mechanism design for knee orthoses.

Control system design of transfemoral prosthesis is an overly complex problem requiring separate solutions to each mode of operation. In other words, each mode of operation has a dedicated control strategy or set of control parameters. To add to this complexity, even the simple task of walking on level ground mandates further decomposition. Currently, prostheses researchers decompose the level walking gait cycle into several states, each with its own set of control parameters. The number of parameters ranges from 12-22 per joint. This set of parameters would then have to be tuned for each user, making user customization of powered prostheses tedious. Moreover, the lack of a guideline on tuning these parameters further complicates user customization, especially considering that these controllers will be tuned by clinicians who generally lack knowledge on control system design. The first contribution of this work was a level walking control framework for transfemoral prostheses with fewer tuning parameters (3-7 per joint). This result was achieved by varying the control parameters as functions of the gait progress. These functions were determined through data-driven approaches involving a least squares fit to healthy human walking data. The proposed controller was tested with a young amputee. The results showed that employing continuous control parameter functions not only reduces the number of tuning parameters, but also improves the consistency of walking. Going forward, improvements to the current gait progress estimation schemes should be made. Doing so would greatly improve the results presented in this work. Current estimation schemes do not perform well at lower walking speeds. Further, they also define the instant of toe-off to be around 60% of the gait cycle and thus cannot account for real time variations in toe-off.

As stated earlier, the controllers vary with each mode of operation. For example, walking on

upslopes requires a different set of control parameters vs. walking on level terrain. Thus, user customization of current transfemoral prostheses controllers requires tuning parameters for each possible slope angle (i.e. -10°, -5°, +5°, and so on). Much like the case with level walking controllers, sloped walking controllers do not have any guidelines for tuning parameters. The primary limiting factor for prescribing any such guidelines is the lack of a relationship between the control parameters and the slope angle. The second contribution of this work fills the aforementioned gap in knowledge. This work proposes: (i) a set of basis functions spanning the required control parameters for all sloped conditions and (ii) a mapping from the slope angle to the weights for linearly combining the basis functions. With the proposed framework, one can now design a controller for any given slope angle. This work also includes a thorough tuning regime for the proposed framework. The controller was tested with an amputee at three slope conditions: -5°, 0°, and +5°. The results portrayed trends found in healthy human walking, deeming this control scheme a success. This work recommends studying the impact of toe joint stiffness on the generated gait kinetics and kinematics under the proposed control scheme. While the prosthesis used in this study consisted of a toe joint, the joint stiffness was fixed. Currently, it is unknown whether the proposed tuning protocol can accommodate for varying toe stiffness. Furthermore, as stated in Chapter 2, the instants of heel-off and toe-off vary with the slope angle. Current gait progress estimation schemes do not consider these slope induced variations. Further research in this area would improve the results of the proposed sloped walking control framework.

On the mechanical design front, a primary area of concern is the mismatch between the assistive device's and human's joint axis. Such axis mismatch leads to device migration, heightened interaction forces, and long donning time. While some researchers have attempted to solve this problem using self-aligning joint mechanisms, their results are limited. None compare their designs against conventional joint mechanisms, leading to a lack of consensus on the performance of such mechanisms in the field of human rehabilitation. The final contribution of this work is a novel self-aligning knee mechanism for orthoses. This design employs allowances at the cuffs of the orthoses, enabling the mechanism's axis of rotation to self-align with a human's joint axis.

The proposed mechanism was compared against conventional designs in a $n = 10$ human subject trial. The results showed that the proposed self-aligning design significantly reduces both device migration and interaction forces. Adopting the proposed design in orthoses would make the device compatible with a wider user base than the state-of-the-art mechanisms, thus easing user customization of orthoses. Moving forward, this work recommends testing a rigid version of the proposed design and investigating actuated versions of the design. A preliminary design for said rigid orthosis has been detailed in Chapter 5. Other avenues for future work include extending this design to the three-dimensional space and customizing the design to account for abnormalities resulting from injuries.

In conclusion, the design of lower limb assistive devices is a multifaceted problem requiring solutions to both mechanical and control system design. While contributions in both realms are required and appreciated, care must be paid to the practicality of said contributions (i.e., whether the end users of the products can fully utilize and modify the contributions to satisfy their specific needs). Unfortunately, there is a lack of attention paid in this regard, which limits the public usage of many lower limb assistive devices. This work was aimed at shining a light on these research gaps and lays the groundwork for better user customization of lower limb assistive devices. It is hoped that other researchers will follow suit and address other concerns regarding user customization.

REFERENCES

[1] L. Kraus, "2016 Disability Statistics Annual Report," tech. rep., University of New Hampshire, Durham, 2017.

[2] K. Ziegler-Graham, E. J. MacKenzie, P. L. Ephraim, T. G. Travison, and R. Brookmeyer, "Estimating the Prevalence of Limb Loss in the United States: 2005 to 2050," *Archives of Physical Medicine and Rehabilitation*, vol. 89, pp. 422–429, mar 2008.

[3] National Spinal Cord Injury Statistical Center, "Spinal Cord Injury Facts and Figures at a Glance," tech. rep., National Spinal Cord Injury Statistical Center, Birmingham, 2018.

[4] K. R. Kaufman, S. Frittoli, and C. A. Frigo, "Gait asymmetry of transfemoral amputees using mechanical and microprocessor-controlled prosthetic knees," *Clinical Biomechanics*, vol. 27, pp. 460–465, jun 2012.

[5] H. M. Herr and A. M. Grabowski, "Bionic ankle–foot prosthesis normalizes walking gait for persons with leg amputation," *Proceedings of the Royal Society B: Biological Sciences*, vol. 279, no. 1728, pp. 457–464, 2012.

[6] M. Goldfarb, "Consideration of powered prosthetic components as they relate to microprocessor knee systems," *JPO: Journal of Prosthetics and Orthotics*, vol. 25, no. 4S, pp. P65–P75, 2013.

[7] B. J. Hafner and R. L. Askew, "Physical performance and self-report outcomes associated with use of passive, adaptive, and active prosthetic knees in persons with unilateral, transfemoral amputation: Randomized crossover trial," *Journal of Rehabilitation Research and Development*, vol. 52, no. 6, pp. 677–700, 2015.

[8] D. C. Morgenroth, M. Roland, A. L. Pruziner, and J. M. Czerniecki, "Transfemoral amputee intact limb loading and compensatory gait mechanics during down slope ambulation and the effect of prosthetic knee mechanisms," *Clinical Biomechanics*, vol. 55, pp. 65–72, jun 2018.

[9] E. J. Wolf, V. Q. Everding, A. L. Linberg, B. L. Schnall, J. M. Czerniecki, and J. M. Gambel, "Assessment of transfemoral amputees using C-leg and Power Knee for ascending and descending inclines and steps," *Journal of Rehabilitation Research and Development*, vol. 49, no. 6, pp. 831–842, 2012.

[10] S. K. Au, H. Herr, J. Weber, and E. C. Martinez-Villalpando, "Powered ankle-foot prosthesis for the improvement of amputee ambulation," in *2007 29th Annual International Conference of the IEEE Engineering in Medicine and Biology Society*, pp. 3020–3026, Aug 2007.

[11] T. Lenzi, M. Cempini, J. Newkirk, L. J. Hargrove, and T. A. Kuiken, "A lightweight robotic ankle prosthesis with non-backdrivable cam-based transmission," in *2017 International Conference on Rehabilitation Robotics (ICORR)*, pp. 1142–1147, July 2017.

[12] E. C. Martinez- Villalpando, J. Weber, G. Elliott, and H. Herr, "Design of an agonist-antagonist active knee prosthesis," in *2008 2nd IEEE RAS EMBS International Conference on Biomedical Robotics and Biomechatronics*, pp. 529–534, Oct 2008.

[13] F. Sup, A. Bohara, and M. Goldfarb, "Design and Control of a Powered Transfemoral Prosthesis," *The International Journal of Robotics Research*, vol. 27, pp. 263–273, feb 2008.

[14] N. Thatte and H. Geyer, "Towards local reflexive control of a powered transfemoral prosthesis for robust amputee push and trip recovery," in *2014 IEEE/RSJ International Conference on Intelligent Robots and Systems*, pp. 2069–2074, Sep. 2014.

[15] M. Windrich, M. Grimmer, O. Christ, S. Rinderknecht, and P. Beckerle, "Active lower limb prosthetics: a systematic review of design issues and solutions," *Biomedical Engineering Online*, vol. 15, no. 3, p. 140, 2016.

[16] H. Zhao, J. Horn, J. Reher, V. Paredes, and A. D. Ames, "First steps toward translating robotic walking to prostheses: a nonlinear optimization based control approach," *Autonomous Robots*, vol. 41, no. 3, pp. 725–742, 2017.

[17] V. Azimi, T. Shu, H. Zhao, E. Ambrose, A. D. Ames, and D. Simon, "Robust control of a powered transfemoral prosthesis device with experimental verification," in *2017 American Control Conference (ACC)*, pp. 517–522, May 2017.

[18] T. Elery, S. Rezazadeh, C. Nesler, J. Doan, H. Zhu, and R. D. Gregg, "Design and benchtop validation of a powered knee-ankle prosthesis with high-torque, low-impedance actuators," in *2018 IEEE International Conference on Robotics and Automation (ICRA)*, pp. 2788–2795, May 2018.

[19] A. F. Azocar, L. M. Mooney, L. J. Hargrove, and E. J. Rouse, "Design and characterization of an open-source robotic leg prosthesis," in *2018 7th IEEE International Conference on Biomedical Robotics and Biomechatronics (Biorob)*, pp. 111–118, Aug 2018.

[20] M. Talaty, A. Esquenazi, and J. E. Briceno, "Differentiating ability in users of the ReWalk^{TM} powered exoskeleton: An analysis of walking kinematics," in *2013 IEEE 13th International Conference on Rehabilitation Robotics (ICORR)*, pp. 1–5, IEEE, jun 2013.

[21] H. A. Quintero, R. J. Farris, and M. Goldfarb, "A Method for the Autonomous Control of Lower Limb Exoskeletons for Persons With Paraplegia," *Journal of Medical Devices*, vol. 6, p. 041003, oct 2012.

[22] R. Little and R. Alexander Irving, "Self contained powered exoskeleton walker for a disabled user," sep 2015.

[23] R. Griffin, T. Cobb, T. Craig, M. Daniel, N. van Dijk, J. Gines, K. Kramer, S. Shah, O. Siebinga, J. Smith, and P. Neuhaus, "Stepping Forward with Exoskeletons: Team IHMC's Design and Approach in the 2016 Cybathlon," *IEEE Robotics & Automation Magazine*, vol. 24, pp. 66–74, dec 2017.

[24] N. Evans, C. Hartigan, C. Kandilakis, E. Pharo, and I. Clesson, "Acute Cardiorespiratory and Metabolic Responses During Exoskeleton-Assisted Walking Overground Among Per-

sons with Chronic Spinal Cord Injury," *Topics in Spinal Cord Injury Rehabilitation*, vol. 21, pp. 122–132, mar 2015.

[25] A. S. Gorgey, "Robotic exoskeletons: The current pros and cons," *World Journal of Orthopedics*, 2018.

[26] B. Chen, H. Ma, L.-Y. Qin, F. Gao, K.-M. Chan, S.-W. Law, L. Qin, and W.-H. Liao, "Recent developments and challenges of lower extremity exoskeletons," *Journal of Orthopaedic Translation*, vol. 5, pp. 26–37, apr 2016.

[27] Y. Wen, J. Si, A. Brandt, X. Gao, and H. H. Huang, "Online reinforcement learning control for the personalization of a robotic knee prosthesis," *IEEE Transactions on Cybernetics*, vol. 50, no. 6, pp. 2346–2356, 2020.

[28] G. Colombo, S. Filippi, C. Rizzi, and F. Rotini, "A new design paradigm for the development of custom-fit soft sockets for lower limb prostheses," *Computers in Industry*, vol. 61, pp. 513–523, aug 2010.

[29] C. Comotti, D. Regazzoni, C. Rizzi, and A. Vitali, "Multi-material design and 3D printing method of lower limb prosthetic sockets," *ACM International Conference Proceeding Series*, vol. 01-02-October-2015, pp. 42–45, oct 2015.

[30] C. Lecomte, A. L. Ármannsdóttir, F. Starker, H. Tryggvason, K. Briem, and S. Brynjolfsson, "Variable stiffness foot design and validation," *Journal of Biomechanics*, vol. 122, p. 110440, jun 2021.

[31] N. P. Fey, G. K. Klute, and R. R. Neptune, "Altering prosthetic foot stiffness influences foot and muscle function during below-knee amputee walking: A modeling and simulation analysis," *Journal of Biomechanics*, vol. 46, pp. 637–644, feb 2013.

[32] O. N. Beck, P. Taboga, and A. M. Grabowski, "Prosthetic model, but not stiffness or height, affects the metabolic cost of running for athletes with unilateral transtibial amputations," *https://doi.org/10.1152/japplphysiol.00896.2016*, vol. 123, pp. 38–48, jul 2017.

[33] M. Regalbuto, J. Rovick, and P. Walker, "The forces in a knee brace as a function of hinge design and placement," *The American Journal of Sports Medicine*, vol. 17, no. 4, pp. 535–543, 1989. PMID: 2782538.

[34] J. M. B. Bertomeu, J. M. B. Lois, R. B. Guillem, Á. P. Del Pozo, J. Lacuesta, C. G. Mollà, P. V. Luna, and J. P. Pastor, "Development of a hinge compatible with the kinematics of the knee joint," *Prosthetics and orthotics international*, vol. 31, no. 4, pp. 371–383, 2007.

[35] T. J. Supan, "Principles of fabrication," in *Atlas of Orthoses and Assistive Devices (Fifth Edition)* (J. B. Webster and D. P. Murphy, eds.), pp. 42–48.e1, Philadelphia: Elsevier, fifth edition ed., 2019.

[36] T. Lee, D. Lee, B. Song, and Y. S. Baek, "Design and control of a polycentric knee exoskeleton using an electro-hydraulic actuator," *Sensors*, vol. 20, no. 1, 2020.

[37] M. F. Kapci and R. Unal, "Design of bio-joint shaped knee exoskeleton assisting for walking and sit-to-stance," in *Wearable Robotics: Challenges and Trends* (M. C. Carrozza, S. Micera, and J. L. Pons, eds.), (Cham), pp. 495–499, Springer International Publishing, 2019.

[38] A. Stienen, E. Hekman, F. van der Helm, and H. van der Kooij, "Self-Aligning Exoskeleton Axes Through Decoupling of Joint Rotations and Translations," *IEEE Transactions on Robotics*, vol. 25, pp. 628–633, jun 2009.

[39] B. Celebi, M. Yalcin, and V. Patoglu, "AssistOn-Knee: A self-aligning knee exoskeleton," in *2013 IEEE/RSJ International Conference on Intelligent Robots and Systems*, pp. 996–1002, IEEE, nov 2013.

[40] V. A. D. Cai, P. Bidaud, V. Hayward, and F. Gosselin, "Self-adjustment mechanisms and their application for orthosis design," *Meccanica 2016 52:3*, vol. 52, pp. 713–728, nov 2016.

[41] B. Choi, Y. Lee, J. Kim, M. Lee, J. Lee, S.-g. Roh, H. Choi, Y.-J. Kim, and J.-y. Choi, "A self-aligning knee joint for walking assistance devices," in *2016 38th Annual International Conference of the IEEE Engineering in Medicine and Biology Society (EMBC)*, pp. 2222–2227, IEEE, aug 2016.

[42] D. A. Winter, *Biomechanics and motor control of human movement*. Wiley, 4 ed., 2009.

[43] J. R. Montgomery and A. M. Grabowski, "The contributions of ankle, knee and hip joint work to individual leg work change during uphill and downhill walking over a range of speeds," *Royal Society Open Science*, vol. 5, no. 8, p. 180550, 2018.

[44] K. R. Embry, D. J. Villarreal, R. L. Macaluso, and R. D. Gregg, "Modeling the kinematics of human locomotion over continuously varying speeds and inclines," *IEEE Transactions on Neural Systems and Rehabilitation Engineering*, vol. 26, pp. 2342–2350, Dec 2018.

[45] K. Embry, D. Villarreal, R. Macaluso, and R. Gregg, "The effect of walking incline and speed on human leg kinematics, kinetics, and emg," 2018.

[46] J. Pons, J. Moreno, F. Brunetti, and E. Roco, "Lower-Limb Wearable Exoskeleton," in *Rehabilitation Robotics*, I-Tech Education and Publishing, aug 2007.

[47] J. Perry, L. A. Boyd, S. S. Rao, and S. J. Mulroy, "Prosthetic weight acceptance mechanics in transtibial amputees wearing the single axis, seattle lite, and flex foot," *IEEE Transactions on Rehabilitation Engineering*, vol. 5, no. 4, pp. 283–289, 1997.

[48] S. Blumentritt, H. W. Scherer, U. Wellershaus, and J. W. Michael, "Design principles, biomechanical data and clinical experience with a polycentric knee offering controlled stance phase knee flexion: a preliminary report," *JPO: Journal of Prosthetics and Orthotics*, vol. 9, no. 1, pp. 18–24, 1997.

[49] D. Romo, "Prosthetic knees," *Physical medicine and rehabilitation clinics of North America*, vol. 11, pp. 595–607, vii, 2000.

[50] N. P. Fey, A. M. Simon, A. J. Young, and L. J. Hargrove, "Controlling knee swing initiation and ankle plantarflexion with an active prosthesis on level and inclined surfaces at variable walking speeds," *IEEE Journal of Translational Engineering in Health and Medicine*, vol. 2, pp. 1–12, 2014.

[51] R. D. Gregg, T. Lenzi, L. J. Hargrove, and J. W. Sensinger, "Virtual constraint control of a powered prosthetic leg: From simulation to experiments with transfemoral amputees," *IEEE Transactions on Robotics*, vol. 30, no. 6, pp. 1455–1471, 2014.

[52] V. Paredes, W. Hong, S. Patrick, and P. Hur, "Upslope walking with transfemoral prosthesis using optimization based spline generation," in *2016 IEEE/RSJ International Conference on Intelligent Robots and Systems (IROS)*, pp. 3204–3211, Oct 2016.

[53] A. E. Martin and R. D. Gregg, "Stable, robust hybrid zero dynamics control of powered lower-limb prostheses," *IEEE Transactions on Automatic Control*, vol. 62, no. 8, pp. 3930–3942, 2017.

[54] M. F. Eilenberg, H. Geyer, and H. Herr, "Control of a Powered Ankle–Foot Prosthesis Based on a Neuromuscular Model," *IEEE Transactions on Neural Systems and Rehabilitation Engineering*, vol. 18, no. 2, pp. 164–173, 2010.

[55] J. Blaya and H. Herr, "Adaptive Control of a Variable-Impedance Ankle-Foot Orthosis to Assist Drop-Foot Gait," *IEEE Transactions on Neural Systems and Rehabilitation Engineering*, vol. 12, pp. 24–31, mar 2004.

[56] K. Bhakta, J. Camargo, P. Kunapuli, L. Childers, and A. Young, "Impedance Control Strategies for Enhancing Sloped and Level Walking Capabilities for Individuals with Transfemoral Amputation Using a Powered Multi-Joint Prosthesis," *Military Medicine*, vol. 185, pp. 490–499, 12 2019.

[57] A. Mohammadi and R. D. Gregg, "Variable impedance control of powered knee prostheses using human-inspired algebraic curves," *Journal of Computational and Nonlinear Dynamics*, vol. 14, pp. 1–10, 2019.

[58] N. Anil Kumar, W. Hong, and P. Hur, "Impedance control of a transfemoral prosthesis using continuously varying ankle impedances and multiple equilibria," in *2020 IEEE International Conference on Robotics and Automation (ICRA)*, pp. 1755–1761, 2020.

[59] E. J. Rouse, L. J. Hargrove, E. J. Perreault, and T. A. Kuiken, "Estimation of Human Ankle Impedance During the Stance Phase of Walking," *IEEE Transactions on Neural Systems and Rehabilitation Engineering*, vol. 22, no. 4, pp. 870–878, 2014.

[60] H. Lee, E. J. Rouse, and H. I. Krebs, "Summary of Human Ankle Mechanical Impedance During Walking," *IEEE Journal of Translational Engineering in Health and Medicine*, vol. 4, pp. 1–7, 2016.

[61] A. L. Shorter and E. J. Rouse, "Mechanical Impedance of the Ankle during the Terminal Stance Phase of Walking," *IEEE Transactions on Neural Systems and Rehabilitation Engineering*, vol. 26, no. 1, pp. 135–143, 2018.

[62] W. Hong, V. Paredes, K. Chao, S. Patrick, and P. Hur, "Consolidated control framework to control a powered transfemoral prosthesis over inclined terrain conditions," in *2019 International Conference on Robotics and Automation (ICRA)*, pp. 2838–2844, May 2019.

[63] N. J. Rosenblatt, A. Bauer, D. Rotter, and M. D. Grabiner, "Active dorsiflexing prostheses may reduce trip-related fall risk in people with transtibial amputation," *Journal of Rehabilitation Research & Development*, vol. 51, no. 8, 2014.

[64] D. J. Villarreal and R. D. Gregg, "Unified phase variables of relative degree two for human locomotion," in *Engineering in Medicine and Biology Society (EMBC), 2016 IEEE 38th Annual International Conference of the*, pp. 6262–6267, IEEE, 2016.

[65] W. Hong, N. A. Kumar, and P. Hur, "A phase-shifting based human gait phase estimation for powered transfemoral prostheses," *IEEE Robotics and Automation Letters*, vol. 6, no. 3, pp. 5113–5120, 2021.

[66] Y. Hurmuzlu, C. Basdogan, and J. J. Carollo, "Presenting joint kinematics of human locomotion using phase plane portraits and poincare maps," *Journal of biomechanics*, vol. 27, no. 12, pp. 1495–1499, 1994.

[67] H. Kantz and T. Schreiber, *Nonlinear time series analysis*, vol. 7. Cambridge university press, 2004.

[68] R. Hegger, H. Kantz, and T. Schreiber, "Practical implementation of nonlinear time series methods: The tisean package," *Chaos: An Interdisciplinary Journal of Nonlinear Science*, vol. 9, no. 2, pp. 413–435, 1999.

[69] F. Sup, H. A. Varol, and M. Goldfarb, "Upslope Walking With a Powered Knee and Ankle Prosthesis: Initial Results With an Amputee Subject," *IEEE Transactions on Neural Systems and Rehabilitation Engineering*, vol. 19, pp. 71–78, Feb 2011.

[70] B. E. Lawson, J. Mitchell, D. Truex, A. Shultz, E. Ledoux, and M. Goldfarb, "A Robotic Leg Prosthesis: Design, Control, and Implementation," *IEEE Robotics & Automation Magazine*, vol. 21, no. 4, pp. 70–81, 2014.

[71] N. Anil Kumar, W. Hong, and P. Hur, "Control of a transfemoral prosthesis on sloped terrain using continuous and nonlinear impedance parameters," in *2021 IEEE International Conference on Robotics and Automation (ICRA)*, pp. 3219–3225, 2021.

[72] N. Alexander, G. Strutzenberger, and H. Schwameder, "The use of the gradual yielding mechanism during downhill walking in transfemoral amputee gait–a case study," *ISBS Proceedings Archive*, vol. 35, no. 1, p. 249, 2017.

[73] N. Anil Kumar, S. Patrick, and P. Hur, "Pilot Study on the Needs of Prospective Exoskeleton Users with Impaired Mobility," *Proceedings of IEEE Workshop on Advanced Robotics and its Social Impacts, ARSO*, vol. 2019-October, pp. 106–111, oct 2019.

[74] G. Serrancoli, A. Falisse, C. Dembia, J. Vantilt, K. Tanghe, D. Lefeber, I. Jonkers, J. De Schutter, and F. De Groote, "Subject-Exoskeleton Contact Model Calibration Leads to Accurate Interaction Force Predictions," *IEEE transactions on neural systems and rehabilitation engineering : a publication of the IEEE Engineering in Medicine and Biology Society*, vol. 27, pp. 1597–1605, aug 2019.

[75] B. Pierrat, C. Millot, J. Molimard, L. Navarro, P. Calmels, P. Edouard, and S. Avril, "Characterisation of Knee Brace Migration and Associated Skin Deformation During Flexion by Full-Field Measurements," *Experimental Mechanics*, vol. 55, no. 2, pp. 349–360, 2015.

[76] V. A. D. Cai, P. Bidaud, V. Hayward, and F. Gosselin, "Self-adjustment mechanisms and their application for orthosis design," *Meccanica*, vol. 52, pp. 713–728, feb 2017.

[77] H. Vive, "Hinged Knee Brace - Open Compression Support - Vive Health," 2021.

[78] M. Olinski, A. Gronowicz, and M. Ceccarelli, "Development and characterisation of a controllable adjustable knee joint mechanism," *Mechanism and Machine Theory*, vol. 155, p. 104101, 2021.

[79] D. hai Wang, J. Guo, K.-M. Lee, C. jun Yang, and H. Yu, "An adaptive knee joint exoskeleton based on biological geometries," in *2011 IEEE International Conference on Robotics and Automation*, pp. 1386–1391, 2011.

[80] M. A. Ergin and V. Patoglu, "A self-adjusting knee exoskeleton for robot-assisted treatment of knee injuries," in *2011 IEEE/RSJ International Conference on Intelligent Robots and Systems*, pp. 4917–4922, IEEE, sep 2011.

[81] D. Cai, P. Bidaud, V. Hayward, and F. Gosselin, "Design of Self-Adjucting Orthoses for Rehabilitation," tech. rep.

APPENDIX A

SUPPLEMENTAL DATA

A.1 Control framework for walking with a transfemoral prosthesis on level ground

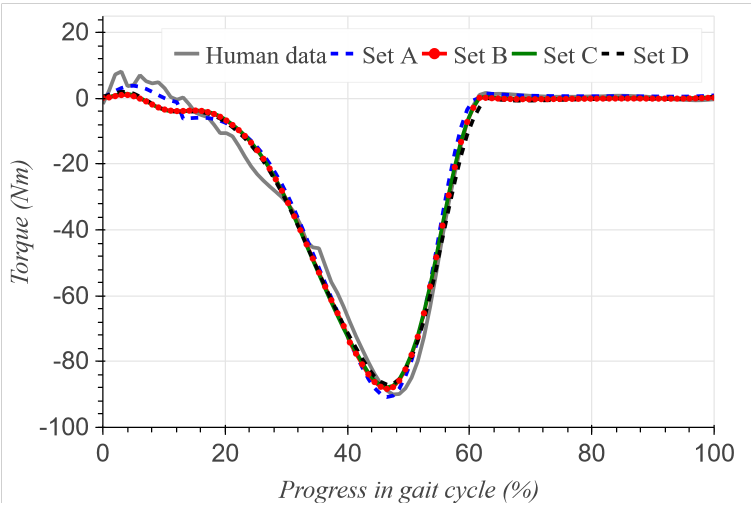

Figure A.1: Optimal torque resulting from control parameter estimation

Table A.1: The coefficients of the polynomial curves for different finite state machines

Stiffness					
Set label	k_4	k_3	k_2	k_1	k_0
Set A	-29870.57	28322.46	-7061.82	586.04	2.21
Set B	-19977.92	17340.71	-3424.51	199.97	0.32
Set C	-19822.71	17146.19	-3333.05	181.16	0.75
Set D	-16520.32	14144.17	-2596.67	136.56	0.00
Damping					
Set label	d_4	d_3	d_2	d_1	d_0
Set A	-22.45	88.08	-76.20	18.76	0.12
Set B	-140.21	261.35	-158.46	31.21	0.12
Set C	-164.32	303.05	-181.22	35.04	0.18
Set D	-171.23	311.36	-182.97	34.53	0.26

Table A.2: The coefficients of the polynomials for continuous control parameters

	Coefficients				
Parameter	$i=4$	$i=3$	$i=2$	$i=1$	$i=0$
			Ankle		
k_i	-15098.92	14008.72	-3209.4435	329.3717	80.
d_i	635.71	-818.08	344.72	-52.46	2.71
θ_{ref_i} -3.54	1.04	1.30	-0.72	0.06	
			Knee		
k_i	9774.90	-4089.81	-4625.69	2156.18	20.0
d_i	86.94	-139.05	64.78	-2.82	0.13
θ_{ref_i} 10.47	2.09	-6.62	1.69	0.03	

A.2 Control framework for walking with a transfemoral prosthesis on sloped terrain

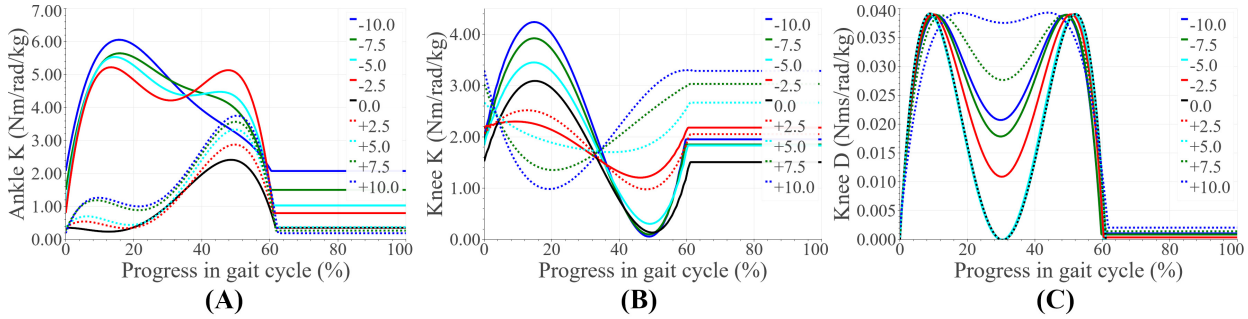

Figure A.2: Joint parameter functions: **(A)** Ankle stiffness, **(B)** Knee stiffness, **(C)** Knee damping

Table A.3: The coefficients of the implemented stiffness and damping polynomials. The word Component has been abbreviated to Comp.

Comp.	k_4	k_3	k_2	k_1	k_0
			Ankle Stiffness (Nm/rad/kg)		
Comp. 1	-108.61	234.61	-160.63	35.23	0.66
Comp. 2	-476.16	493.56	-146.91	14.63	0.52
			Knee Stiffness (Nm/rad/kg)		
Comp. 1	-13.291	-74.669	96.030	-27.672	2.525
Comp. 2	77.418	-41.999	-8.480	2.949	2.317
Comp.	d_4	d_3	d_2	d_1	d_0
			Ankle Damping (Nms/rad/kg)		
Comp. 1	-3.41	5.75	-3.18	0.58	0.00
Comp. 2	1.75	-1.60	0.36	-0.02	0.01
			Knee Damping (Nms/rad/kg)		
Comp. 1	3.905	-4.844	1.622	-0.074	0.001
Comp. 2	-13.022	16.146	-6.402	0.866	0.000

A.3 Self-aligning polycentric mechanism for knee orthosis

Table A.4: Individual details for the final 10 participants

Participant	Mass(kg)	Height(cm)	Age	BMI	Knee Width(cm)	Sex
1	59.3	170.2	28.0	20.5	10.1	M
2	51.0	164.0	28.0	19.0	9.3	F
3	74.7	180.3	27.0	23.0	10.4	M
*4	85.3	177.8	26.0	27.0	10.2	M
5	65.2	172.7	28.0	21.9	9.7	M
6	69.7	169.5	27.0	24.2	11.2	F
7	71.0	170.0	32.0	24.6	11.2	M
8	79.9	172.7	30.0	26.8	11.3	F
9	63.2	166.0	23.0	22.9	9.8	M
10	85.3	170.0	30.0	29.5	12.0	M
Average	70.5	171.3	27.9	23.9	10.5	**F - 3**
Standard deviation	11.2	4.9	2.5	3.2	0.9	**M - 7**

20 leg raises 7min walking 20 leg raises

Figure A.3: Each trial consisted of 20 leg raises, followed by 7 minutes of walking at 1.23 m/s speed, and concluded with another 20 leg raises

Table A.5: Bill of materials for a rigid version of the proposed orthosis design

No.	Part	Purpose	Vendor	Part name	Qty
1	ShoulderBolt	Rotary joint shaft	McMaster	90265A254	4
2	Bushing	Rotary joint	McMaster	2705T129	4
3	M8 insert 10ack	Rotary links	McMaster	94180A504	1
4	Linear bearings	Linear bearings	Misumi	LMU5	10
5	Rotary Shafts	Linear bearings	Misumi	NSFMRT5-40-MD3	10
6	Spring 5 pack	Linear allowances	McMaster	94125K203	6
7	OD 10mm c-clips	Linear bearings	McMaster	98541A118	1
8	M3 screws 10mm	Linear allowances	McMaster	94209A357	1
9	Neoprene sponge	Cuffs	Amazon		1
10	Neoprene rubber	Cuffs	Amazon		1
11	Velcro straps 10pack	Cuffs	Amazon		1
12	M3 screws 8mm	Cuffs	McMaster	94209A356	1
13	M3 Inserts 25pack	Cuffs	McMaster	97164A113	1